DOT/FAA/AR-99/62

Office of Aviation Research
Washington, D.C. 20591

Studies of Time-Phased Vertical and Lateral Gusts: Development of Multiaxis One-Minus-Cosine Gust Model

October 1999

Final Report

U.S. Department of Transportation
Federal Aviation Administration

NOTICE

This document is disseminated under the sponsorship of the U.S. Department of Transportation in the interest of information exchange. The United States Government assumes no liability for the contents or use thereof. The United States Government does not endorse products or manufacturers. Trade or manufacturer's names appear herein solely because they are considered essential to the objective of this report. This document does not constitute FAA certification policy. Consult your local FAA aircraft certification office as to its use.

This report is available at the Federal Aviation Administration William J. Hughes Technical Center's Full-Text Technical Reports page: www.tc.faa.gov/its/act141/reportpage.html in Adobe Acrobat portable document format (PDF).

Technical Report Documentation Page

1. Report No.	2. Government Accession No.	3. Recipient's Catalog No.
DOT/FAA/AR-99/62		

4. Title and Subtitle	5. Report Date
STUDIES OF TIME-PHASED VERTICAL AND LATERAL GUSTS: DEVELOPMENT OF MULTIAXIS ONE-MINUS-COSINE GUST MODEL	October 1999
	6. Performing Organization Code

7. Author(s)	8. Performing Organization Report No.
J.G. Jones	SDL-571-TR-2

9. Performing Organization Name and Address	10. Work Unit No. (TRAIS)
Stirling Dynamics Limited Terminal Buildings Blackbushe Airport Blackwater Camberley Surrey GU17 9LQ	RPD-510
	11. Contract or Grant No.
	DTFA03-98-P-00225

12. Sponsoring Agency Name and Address	13. Type of Report and Period Covered
U.S. Department of Transportation Federal Aviation Administration Office of Aviation Research Washington, DC 20591	Final Report
	14. Sponsoring Agency Code
	ANM-100

15. Supplementary Notes

The Federal Aviation Administration William J. Hughes Technical COTR was Thomas DeFiore. The FAA Technical Advisor was Terry Barnes, NRS on Flight Loads and Aeroelasticity.

16. Abstract

At a Gust Specialists meeting convened by the Federal Aviation Administration (FAA) in 1998, a multiaxis extension of the existing tuned isolated discrete-gust (IDG) method (1-cosine profile) incorporating a pair of vertical and lateral one-minus-cosine gusts was proposed [1,2]. A particular application of this method is the gust response of wing-mounted nacelles. This report presents the theoretical and empirical basis for this gust model, including results from a statistical analysis of measured turbulence data in support of the use of an "amplitude-reduction" factor which relates the magnitudes of the gust components in the multiaxis model to the magnitude of a single (1-cosine) gust in one axis as defined in the current tuned isolated discrete-gust requirement. On this basis, a proposal is made for the possible form of an associated airworthiness rule. Applications of this method to the engine nacelle responses of an Airbus-type aircraft dynamic model are presented and the resulting predicted loads compared with those resulting from the multiaxis PSD method and from a round-the-clock isolated discrete-gust analysis. A statistical analysis is also presented of the engine nacelle loads resulting when the same aircraft dynamic model is subjected to measured turbulence inputs and these loads are compared with the predicted loads resulting from the proposed multiaxis analysis method.

17. Key Words	18. Distribution Statement
Discrete gust, Turbulence, Multiple axis, Wing-mounted nacelles	This document is available to the public through the National Technical Information Service (NTIS), Springfield, Virginia 22161.

19. Security Classif. (of this report)	20. Security Classif. (of this page)	21. No. of Pages	22. Price
Unclassified	Unclassified	61	

TABLE OF CONTENTS

LIST OF FIGURES

LIST OF TABLES

LIST OF ACRONYMS

CAADRP	Civil Aircraft Airworthiness Data Recording Programme
DERA	Defence Evaluation and Research Agency
IDG	Isolated Discrete-Gust
IDGRC	Isolated Discrete-Gust Round-The-Clock
PSD	Power Spectral Density
PSDMA	Power Spectral Density Multiaxis
SDG	Statistical Discrete-Gust

EXECUTIVE SUMMARY

At a Gust Specialists meeting convened by the Federal Aviation Administration (FAA) in 1998, a multiaxis extension of the existing tuned isolated discrete-gust (IDG) method (1-cosine profile) incorporating a pair of vertical and lateral one-minus-cosine gusts was proposed [1,2]. A particular application of this method is the gust response of wing-mounted nacelles. This report presents the theoretical and empirical basis for this gust model, including results from a statistical analysis of measured turbulence data in support of the use of an "amplitude-reduction" factor which relates the magnitudes of the gust components in the multiaxis model to the magnitude of a single (1-cosine) gust in one axis as defined in the current tuned isolated discrete-gust requirement. On this basis, a proposal is made for the possible form of an associated airworthiness rule. Applications of this method to the engine nacelle responses of an Airbus-type aircraft dynamic model are presented and the resulting predicted loads compared with those resulting from the multiaxis PSD method and from a round-the-clock isolated discrete-gust analysis. A statistical analysis is also presented of the engine nacelle loads resulting when the same aircraft dynamic model is subjected to measured turbulence inputs and these loads are compared with the predicted loads resulting from the proposed multiaxis analysis method.

1. INTRODUCTION.

In reference 1 a multiaxis extension of the existing tuned isolated discrete-gust (IDG) method (1-cosine profile) was proposed which incorporates multiaxis gust patterns that comprise a pair of vertical and lateral one-minus-cosine gusts, one in each axis. To determine maximum multiaxis loads, the vertical and lateral gust responses are tuned independently. Each gust component has its own tuned gradient distance, and the two gust components, which may be sequential or may overlap, are time-phased or time-delayed such that the individual maximum peak responses occur at the same instant. The resulting design load is taken to be the maximum of the loads arising from the standard single-axis and multiple-axis analyses.

The multiaxis gust model incorporates an amplitude-reduction factor analogous to associated factors in the SDG1 method [3,4] such that the probability of meeting the proposed multiaxis gust pattern is the same as that of meeting a single (1-cosine) gust in one axis, as defined in the current IDG requirement.

The new method for multiaxis gust analysis is intended to be complementary to, rather than to replace, the isolated discrete-gust round-the-clock (IDGRC) analysis, and the proposed form of an associated airworthiness rule requires both methods to be applied.

The steps to be taken in applying the multiaxis model are as follows [1]:

a. Using (1-cosine) gust profiles, perform independent analyses as in the current IDG requirement to identify the single largest response peaks in the vertical and lateral axes together with their associated tuned inputs. Denote the tuned gust components in the two axes by $g_1(t)$ and $g_2(t)$ and the magnitudes of their associated tuned response peaks by x_1 and x_2.

b. As described below, scale the overall magnitude of the gust pair such that the occurrence of the multiaxis combination of gusts has the same probability of occurrence as a single (1-cosine) gust as specified in the current IDG airworthiness requirement, and determine the relative amplitudes of the two gust components so as to maximise the combined response.

   As will be shown in section 3, to a first approximation (based on Gaussian random process theory), the scaled gusts in the optimum combination are respectively

$$\frac{x_1\, g_1(t)}{\sqrt{x_1^2+x_2^2}} \quad and \quad \frac{x_2\, g_2(t)}{\sqrt{x_1^2+x_2^2}} \tag{1}$$

   and the resulting overall maximised response is given by

$$\sqrt{x_1^2+x_2^2} \tag{2}$$

It may be noted that in the particular situation in which $x_1 = x_2$, the prefactors on $g_1(t)$ and $g_2(t)$ in equation 1 take the value $1/\sqrt{2}$.

c. Following a standard procedure in the SDG method [3,4], apply a further amplitude-reduction factor P (< 1) to equations 1 and 2 above to allow for non-Gaussian properties of extreme turbulence which are associated with phase correlations between different frequency components. The proposed numerical value for this factor is:

$$P=\sqrt{\frac{e_4}{e_2}}=0.85 \qquad (3)$$

where e_2 and e_4 are energy factors used in the SDG1 method whose numerical values are given in equation 1.1 of reference 4.

d. Compare the resulting multiaxis loads with those resulting from an isolated discrete-gust analysis (in both vertical and lateral axes) and with those resulting from an isolated discrete-gust round-the-clock analysis and base the design load on the greatest of these.

In the remainder of this report, the theoretical and empirical basis for use of equations 1 to 3 is presented, and the results of a statistical study which supports the use of the numerical factor in equation 3 are described.

2. PROBABILITY DISTRIBUTIONS FOR MULTIPLE-AXIS DISCRETE GUSTS.

In the following, probability distributions for multiple-axis discrete gusts are introduced in two steps. In the first step, section 2.1, the probabilities for single-axis isolated gusts are associated with a generalised energy, which is derived from Gaussian random process theory. This relationship is sufficient to describe how, for a given level of probability, the amplitude of a discrete gust of given shape varies with its scale or gradient distance. In section 2.2 it is shown how the concept of generalised energy can be extended to the multiple-axis situation, and it is demonstrated how, using this concept, the amplitude of a prescribed single gust in one axis can be related to the amplitudes of the two components in a multiaxis gust pattern at the same level of probability.

Whilst the generalised energy (section 2.1) provides a baseline first approximation, empirical studies have shown that for discrete gusts in real atmospheric turbulence of the severe to extreme intensities relevant to design loads, a further step is required in which the number of gust components in a gust pattern modifies the first approximation. This further step, described in section 4, involves the introduction of complexity factors which take into account the non-Gaussian nature of the turbulence associated with *phase correlations* that are neglected in the first (Gaussian) approximation. When applied to the multiaxis model, these factors reduce to a single amplitude-reduction factor P, equation 3, which takes into account the phase correlations between the vertical and lateral gust components.

2.1 PROBABILITY AND GENERALISED ENERGY.

Studies of the relationship between deterministic and stochastic representations of a fluctuating process [5,6] have clarified the way in which the probability of meeting a gust pattern of arbitrary shape can be expressed in terms of its generalised energy. Specifically, to an approximation consistent with stationary Gaussian random process theory, the probability of encountering a specific deterministic realisation v(t) depends upon the generalised energy:

$$U = \frac{1}{2}\int_0^\infty \frac{|V(i\omega)|^2}{\varphi(\omega)}\,d\omega \tag{4}$$

where $V(i\omega)$ is the Fourier transform of $v(t)$ and $\varphi(\omega)$ is a frequency weighting function that may be identified with the power spectral density of a related Gaussian random process [5, 6].

The generalised energy U, equation 4, can equally be expressed in the time plane [6]. Here we shall only be concerned with the case in which it is applied to a family of discrete gusts with individual profiles that take the standard (1-cosine) form and equi-probable gusts that satisfy the one-sixth power law for the relationship between gust amplitude and gust gradient distance over a specified range of gradient distances. If, over this range, we take $\varphi(\omega)$ to be proportional to $\omega^{-4/3}$, then the generalised energy U, equation 4, takes the form [6]:

$$U = k\frac{v^2}{H^{1/3}} \tag{5}$$

where k is a constant and v and H are respectively the peak gust amplitude and the gust gradient distance. Clearly, gusts for which v is proportional to $H^{1/6}$ take the same value of U and hence have the same probability. Different values of k in equation 5 correspond to different levels of probability

2.2 MULTIAXIS CASE.

The relationship between generalised energy, equation 4, and probability generalises to the multiaxis case in which $v(t)$ becomes a vector with orthogonal components $v_1(t)$ and $v_2(t)$. On account of orthogonality, the generalised energy which determines the overall probability of the deterministic vector $v(t)$ equals the sum of the energies of the components $v_1(t)$ and $v_2(t)$. If we consider the case in which the profiles of the individual components take the standard (1-cosine) form in each axis, then the contributions U_1 and U_2 from each axis to the generalised energy take the form of equation 5:

$$U_1 = k_1\frac{v_1^{\,2}}{H_1^{1/3}} \tag{6}$$

$$U_2 = k_2\frac{v_2^{\,2}}{H_2^{1/3}}$$

and a prescribed level of probability for the multiaxis pattern corresponds to a prescribed value of $U_1 + U_2$.

3. MULTIAXIS LOADS.

We first derive the equations 1 and 2 for multiaxis loads on the basis of the theory in section 2.2.

Following the steps outlined in section 1, a single-axis analysis is first performed in each axis using a (1-cosine) gust as in the current requirement. The particular family of gusts follows a specified one-sixth law. This will correspond to a particular value of k in equation 5 and hence of the generalised energy U. We suppose that the resulting peak loads are x_1 and x_2 and that the associated gust profiles are $g_1(t)$ and $g_2(t)$.

Next we consider multiaxis patterns with a (1-cosine) gust component in each axis. As described in section 2.2, to retain the same overall level of probability, the sum U_1+U_2 of the energies in the two axes (equation 6) is constrained to take the value U corresponding to the single-axis case. That is, we may distribute U according to

$$U_1=\alpha U \quad \text{and } U_2=(1-\alpha)U \text{ , where } 0 \le \alpha \le 1 \tag{7}$$

For any specified value of α, the maximum load that can be caused by the gust in the first axis is $\sqrt{\alpha}\, x_1$ and in the second axis $\sqrt{1-\alpha}\, x_2$ with the associated gust profiles being $\sqrt{\alpha}\; g_1(t)$ and $\sqrt{1-\alpha}\; g_2(t)$. For this value of α, the maximum overall load is

$$L=\sqrt{\alpha}\, x_1+\sqrt{1-\alpha}\, x_2 \tag{8}$$

and will be achieved when the two gusts are time-phased such that the associated peak component loads occur at the same instant.

It remains to choose α so as to maximise L, equation 8. It is easily verified that the maximum occurs when

$$\alpha=\frac{x_1^2}{x_1^2+x_2^2} \tag{9}$$

Combining equations 8 and 9, it follows that the maximum response is given by equation 2, and the associated component gust inputs are given by equation 1, section 1.

The final step, to be discussed in section 4, is to introduce the amplitude-reduction factor P, equation 3, into the multiaxis gust model. This factor is to be applied directly, both to the maximised response, equation 2, and to the gust component time histories, equation 1.

4. PHASE CORRELATION AND COMPLEXITY FACTORS.

The theory outlined in previous sections rests on the same basic principles as Power Spectral Density (PSD)-based matched-filter theory. In particular it assumes implicitly that phase correlations between Fourier components, whether in the same axis or in different axes, are uncorrelated. To take into account such phase correlations, the SDG method introduces empirically based complexity factors which, for a prescribed level of probability, determine the relative amplitudes of single discrete gusts and gust patterns comprising multiple components.

In the case of the SDG1 method [3,4], these complexity factors are implemented by means of energy-reduction factors, or e-factors, in which the concept of generalised energy, as defined above, is retained, but a reduction in total generalised energy is incorporated in going from a single-component gust to a pattern comprising multiple-gust components. Until now there has been empirical evidence for this reduction only when the individual gust components occur in the same axis [7,8].

To cover the multiaxis situation with gust components in different axes, further studies have been performed to justify the use of analogous factors. The method of analysis of measured data is described in sections 6.1 and 6.2 and results are presented in section 7. The resulting amplitude-reduction factor P, equation 3, applied to multiple-axis gust patterns in effect takes into account the phase correlations between Fourier components in the two axes.

5. EMPIRICAL BASIS FOR COMPLEXITY FACTORS.

5.1 THE TWO DATA SOURCES.

Two sources of measured data, to be described, play complementary roles in the empirical basis for the proposed multiaxis gust model. The Civil Aviation Authority Data Reporting Program (CAADRP) data, section 5.2, incorporate special events associated with aircraft normal acceleration and are recorded during routine operational flying. However, these events contain no information concerning the lateral gust component.

The Gnat data, section 5.3, on the other hand, were obtained by a specially instrumented research aircraft and comprise simultaneous measurements of the vertical and lateral gust components. The data were obtained under a wide range of atmospheric conditions and types of underlying terrain but were limited to the lowest 1000 ft of the atmosphere.

5.2 THE CAADRP DATA.

The basis for the complexity factors lies in the p factors used in the original SDG method [9,10]. With increasing pattern complexity, as defined by the number n of elementary components in the pattern, these p factors provide a means for scaling the amplitudes of the individual gust components so that the overall pattern retains a constant level of probability. As described in reference 7, a study of severe gust encounters recorded during routine commercial operations by the CAADRP programme led to the conclusion that, for gust patterns containing multiple components, the p factors derived from such severe gust encounters are systematically smaller in magnitude than the values that had been derived previously from studies of encounters with

turbulence of moderate intensity and which had also been shown to give approximate equivalence with the PSD method. The p factors derived for a particular severe turbulence encounter are given in equation 4 of reference 7, and the results for all the encounters analysed are presented in figure 23 of reference 7.

Subsequently, the p factors were converted into equivalent energy-reduction factors, or e-factors, and used in the algorithms for SDG1 analysis [3,4]. These factors are defined such that, for a gust pattern comprising n elementary ramp-shaped components, the total generalised energy, section 2.1, is proportional to e_n, where e_1 is normalised to be unity.

The p factors used as a basis for the analysis in references 3 and 4 were derived by curve fitting to the results at the higher levels of intensity in figure 23 of reference 7. Specifically, the derived values were

$$p_1 = 1.0, \quad p_2 = 0.705, \quad p_4 = 0.420 \tag{10}$$

These values were derived [7] using the assumption of equipartition of probability amongst the elementary gust components. Interpreted in terms of SDG1 for a pattern of n components, this corresponds to the equipartition of generalised energy amongst the n components. The energy available for each component is thus proportional to e_n/n. The associated amplitude of each gust component is thus proportional to $(e_n/n)^{1/2}$.

As shown in previous studies of the relationship between p factors and the energy of a gust pattern, in reference 10 for example, in the original SDG method it was necessary to introduce, for all gust patterns with $n>1$ components, an empirical factor of $(0.88)^{-1}$ on p_n to compensate for the reduction in the worst-case response of a system due to the constraint introduced by equipartition. The use of this factor is to be seen in equation 15 of reference 10.

In consequence, the relationship between the amplitude p factors derived from reference 7 and the energy-reduction, or e- factors, used in SDG1 is as follows:

for $n = 1$,

$$p_1 = e_1 = 1 \tag{11}$$

for $n > 1$,

$$p_n = \frac{1}{0.88}\sqrt{\left(\frac{e_n}{n}\right)} \tag{12}$$

It may be noted that if we make the assumption that $e_n = 1$ for all n, as is the case for SDG2 whose purpose is approximate equivalence with the PSD method, equation 12 above agrees exactly with equation 15 of reference 10.

If the numerical values in equation 10 are substituted into equation 12, the following energy-reduction factors as used in SDG1 [4] are obtained:

$$e_1 = 1,\ e_2 = 0.77,\ e_4 = 0.55 \tag{13}$$

In particular, since a (1-cosine) gust comprises two ramp components, such as an up ramp followed immediately by a down ramp, to achieve equal probability between a single (1-cosine) gust and a pair of sequential (1-cosine) gusts in the same axis a reduction in generalised energy of e_4/e_2 is required. Since the energy involves the square of the velocities, as in equation 6, this corresponds to an amplitude-reduction factor of $\sqrt{\frac{e_4}{e_2}} = 0.85$.

In reference 2, preliminary evidence was presented in support of the use of this same factor to achieve equal probability between a single (1-cosine) gust and a pair of sequential (1-cosine) gusts in different axes, equation 3.

The confirmation of this result is the purpose of the analysis of Gnat data, to be described in section 6.

5.3 THE GNAT DATA.

An aircraft based at the Royal Aircraft Establishment, Bedford, England (now Defence Evaluation and Research Agency, DERA), was used in a gust measurement programme [11,12] to collect samples of atmospheric turbulence-velocity at altitudes up to about 1000 ft. using special instrumentation to remove the effects of aircraft motion. Measurements were made under a range of atmospheric conditions over various types of terrain and at a number of heights.

The instrumentation carried included pairs of Conrad Yawmeters and miniature pitot tubes on an extended nose probe. Calibration incorporated results obtained from wind tunnel tests and allowed airflow direction and speed at the nose probe to be derived from data from the yawmeters and pitot tubes. The calculation of time histories of turbulence-velocity involved correcting for instrument dynamic behaviour and removing the effects of sensor motion. A summary of the data processing, including details of the digital filters used to make corrections for pneumatic pipe dynamics and a review of the method used to remove effects of sensor motion, is given in reference 11.

The three measured components of turbulence-velocity are referenced with respect to an aircraft body-axis system and are denoted by u_g (head-on component), v_g (side component), and w_g (normal component). Although they are not strictly components in earth axes, in practice the restriction to a nominally straight track, the fairly small pitch attitudes reached in the turbulence-measuring runs and the pilot's efforts to keep wings level mean that the normal component is very nearly the same as the earth-based vertical component.

The x direction, in body axes, is along the aircraft forward path; and the turbulence field is traversed at the aircraft flight speed, typically 180 m/s. Although the turbulence fluctuations are measured as functions of time, the usual (Taylor's) frozen-field hypothesis has been used to

convert them to functions of position in space. For the purposes of the present study, all runs have been subsampled, using interpolation in combination with an anti-aliasing filter, to a common spatial sampling interval of 2 m.

Although high-quality data covering a wide range of conditions are available, these exclude several typical sources of turbulence that can cause severe structural loads, such as conditions near storm tops or layers of clear air turbulence associated with wave perturbations of stable layers.

Nevertheless, the view is taken that the wide range of atmospheric conditions and degrees of terrain roughness covered by these flight measurements provide an adequate database, for the purposes of this study, to investigate the relationships between single-axis and multiple-axis gust patterns in severe turbulence. Twenty-five turbulence-velocity records have been selected for analysis in the present study on the basis of having similar characteristics to those observed in the CAADRP programme. In particular, the selected turbulence time-histories have a high degree of intermittency and have intensities of the same order as, and in some cases greater than, those of the turbulence encounters involved in the CAADRP analysis in reference 7. Some examples are illustrated in figure 1.

6. ANALYSIS OF GNAT DATA.

6.1 METHOD OF STATISTICAL ANALYSIS.

A method for analysing atmospheric turbulence data which extracts localised structure at multiple scales, in the form of discrete ramp-shaped gusts, has been described in references 11 and 12. The method, which may be identified as a form of wavelet analysis, involves the use of a correlation filter which is translated with respect to the data and also dilated (zoomed) to extract information at different scales. Localised events or structures are then detected by the identification of peaks (maxima or minima) in the resulting filter output.

As described in reference 12, the method assumes that the structures to be detected can be represented in terms of ramp-shaped gusts, any measured turbulence sample being represented as the sum of such structures and a residual error, or noise, term. Optimum detection then involves finding the structures which minimise the variance of the error term.

It is further described in reference 12 how the assumption of a particular analytical form for the power spectral density of the noise leads to the establishment of a relationship between the shape of the structure to be detected and the form of the filter for optimum detection. On this basis, it is shown that, under the assumption that the power spectral density of the noise can be approximated over the bandwidth of the structure to be detected by a power law of the form $|\omega|^{-2}$, the optimum filter to detect ramp-shaped gusts takes the form of a combined smoothing and differencing filter. The analysis is thus based upon a filter of the form

$$T(y,L)=\int H(x-y,L)\Delta u(x,L)dx \qquad (14)$$

applied to a velocity component u(y), where

$$\Delta u(y,L)=u\left(y+\frac{L}{2}\right)-u\left(y-\frac{L}{2}\right) \tag{15}$$

is the differencing filter. In equation 14, $H(x,L)$ is a smoothing function which introduces a weighted average over a distance of order L.

The function $T(y,L)$, equation 14, can equally be written in the alternative form

$$T(y,L)=L^{-1}\int F\left(\frac{x-y}{L}\right)u(x)dx \tag{16}$$

which expresses the convolution of the measured velocity component $u(x)$ with a translated and scaled-filter $F(x)$. $F(x)$ is itself the convolution of a pair of delta functions of opposite sign and unit separation (representing the differencing operation) with the averaging function $H(x,1)$ over unit distance.

In the statistical analysis of measured turbulence data [12], local maxima and minima in $T(y,L)$, with respect to y at given L, are identified. For values of L separated by octave intervals, cumulative distributions are derived in the form of the number $n(L,X)$, per unit distance y, of local extrema in $T(y,L)$ having magnitude greater than X. As demonstrated in reference 12, measured exceedance rates $n(L,X)$ corresponding to different values of L can be used in particular to demonstrate the one-sixth scaling law for the dependence of gust amplitude upon scale, or gradient distance, L.

6.2 MEASUREMENT OF MULTIAXIS AMPLITUDE-REDUCTION FACTOR *P*.

It requires only a simple extension of the above method to detect gust patterns represented as linear combinations of ramp-shaped gusts by means of associated linear combinations of smoothing and differencing filters and, hence, to measure associated statistical distributions. As for single ramps, multiple-ramp patterns are detected as local maxima and minima in the associated filter output. This is true in particular of gust profiles of the standard (1-cosine) shape, which can be represented as an up ramp followed by a down ramp, and of combinations of (1-cosine) gusts. Furthermore, the method extends to multiaxis situations such as that in which the event to be detected comprises one (1-cosine) gust in one axis and another in an orthogonal axis.

Extending the discrete gust analysis method of references 11 and12, for multiple-ramp patterns with n components, the exceedance rate for local maxima and minima takes the form:

$$n(L,X)=\frac{a_n\alpha}{\lambda L}exp\left[-\frac{X}{p_n\beta L^k}\right] \tag{17}$$

where a_n and p_n are factors which take the value unity when $n=1$.

As in equation 12, the p_n can be expressed in terms of the energy-reduction factors e_n. Equation 17 can thus be rewritten as:

$$n(L,X)=\frac{a_n \alpha}{\lambda L} exp\left[-\frac{\sqrt{n}\,X}{\sqrt{e_n}\,\beta\,L^k}\right] \tag{18}$$

and rearranged in the form:

$$ln[Ln(L,x)]=ln\frac{a_n \alpha}{\lambda}-\frac{\sqrt{n}\,X}{\sqrt{e_n}\,\beta L^k} \tag{19}$$

Analysis of a given turbulence record at a specified value of L yields a measured distribution $n(L,X)$ as a function of X. According to equation 19, plotting $ln[Ln(L,X)]$ against X gives points on a straight line whose slope is proportional to $-\sqrt{n/e_n}$.

In this study we are particularly concerned with measurement of the ratio $\sqrt{e_4/e_2}$ for use in equation 3. This is achieved by applying equation 19 to the outputs of two filters, one designed to detect single (1-cosine) gusts and the other to detect pairs of such gusts (one in each of the vertical and lateral axes). Dividing the slope obtained for the gust pair by that obtained for the single (1-cosine) gust gives a measurement of the required quantity:

$$\sqrt{2}\cdot(ratio\ of\ slopes)=\sqrt{\frac{e_4}{e_2}}=P \tag{20}$$

The required slopes have been obtained by least-squares fitting of straight-line segments over specified ranges of amplitude to the measured exceedance rates $n(L,X)$ using log-linear axes. Examples of measured exceedance rates, typical of those from which values of P have been derived in the present study, are illustrated in appendix A.

In the particular situation in which the input is taken to be a Gaussian random process, the energy reduction factors e_n take a theoretical value equal to unity for all n. As will be illustrated in section 7.3 in conjunction with equation 20, this theoretical result provides an empirical check on the validity of the method. An analogous result holds (section 7.3) for signals with random-phase whose power-spectral densities take the same form as those derived from the measured Gnat data. The procedure for generating the required random-phase inputs is described in appendix B.

7. PRESENTATION OF RESULTS.

7.1 CHOICE OF RUNS AND FILTERS.

Twenty-five turbulence-velocity time histories, including both vertical and lateral components, have been selected on the basis of having a high degree of intermittency and include runs of

intensities greater than those of the turbulence encounters involved in the CAADRP analysis [7]. Examples are illustrated in figure 1.

As described in section 6.2, values of P have been derived by comparing the outputs of pairs of filters, one designed to detect single (1-cosine) gusts and the other to detect multiple-axis combinations of such gusts (one in each of the vertical and lateral axes). One example of the pairs of gust patterns that the filters have been designed to detect is shown in figure 2. In this case the single gust, figure 2(a), lies in the vertical (V) axis and the multiple-axis combination, figure 2(b), comprises a vertical gust followed by a lateral gust (VL). Such a pair of filters is denoted by V-VL. Similarly, a pair of filters in which the single gust lies in the lateral (L) axis and the multiple-axis combination comprises a lateral gust followed by a vertical gust (LV) is denoted by L-LV. In all, four such filter pairs have been applied, denoted respectively by V-VL, V-LV, L-LV, and L-VL.

To remove effects of anisotropy in the measured turbulence and to combine situations in which a vertical gust is followed by a lateral gust with those in which the sequence is reversed, the results to be presented have been obtained by averaging results from such filter combinations.

In section 7.2, results are presented first for multiple-axis gust combinations in which the vertical and lateral gust components have the same gradient distance. Subsequently, in section 7.4, results are given for more general situations in which the gust components in the two axes have different gradient distances. In all cases, the pairs of gust components have been analysed over a range of gust separation distances.

In addition to conditions in which the components of a gust pair are sequential, with no overlap, situations with overlapping components have also been analysed. In this overlap case, the two components do not strictly represent two different gusts but, rather, are projections on to the vertical and lateral axes of a complex three-dimensional gust pattern. In particular, in the limiting case in which the overlap is exact, (1-cosine) components in the two axes simply represent projections of a single (1-cosine) gust at some intermediate angle (depending upon the relative amplitudes of the two components) as used in a round-the-clock gust analysis.

7.2 MULTIAXIS GUST COMPONENTS HAVING SAME GRADIENT DISTANCE.

A pattern comprising a pair of gust components having the same gradient distance H, one in each of the vertical and lateral axes, is illustrated in figure 2(b). As shown, the gust lengths AB and CD are equal to $2H$. We introduce the terminology gust separation and gust displacement such that the gust displacement is the distance AC between the positions of onset of the respective gusts and the gust separation is the distance BC between the end of the first gust and the onset of the second gust. The condition illustrated in figure 2(b) is that of sequential, non-overlapping, gust components. However, it follows from the equation $AC = 2H + BC$ that, according to this terminology, when the gust components overlap, i.e., $AC < AB$, the gust separation BC is treated as a negative quantity.

Based on the method of analysis outlined in section 6.2, specifically using equation 20, measured values of the amplitude-reduction factor P, for pairs of gust components having the same

gradient distance and also the same amplitude, are presented in figure 3. These results have been obtained by averaging over 25 turbulence-velocity records, as described in section 5.3.

Values of the amplitude-reduction factor P are shown in figure 3 as a function of the gust-component displacement, defined as in figure 2(b), normalised by the gust length $2H$.

Results are presented in figure 3 for values of the normalised displacement taking values from 0 to 9. Values between 0 and 1 correspond to overlapping gust components. As explained in section 7.1, when the normalised displacement is equal to zero the gust components, having equal gust length, can be interpreted as representing projections of a single (1-cosine) gust at an intermediate angle as used in a round-the-clock gust analysis. For the results illustrated in figure 3, for which the gust components have also been taken to have the same amplitude, this intermediate angle is 45 degrees.

When the normalised displacement is equal to unity, in the notation of figure 2(a) $AC = 2H$ and thus the gust separation AC is equal to zero. That is, the condition of normalised displacement equal to unity corresponds to the case in which the onset of the second gust component occurs exactly at the end point of the first component.

The maximum value of normalised displacement has been taken to be 9. This corresponds to the condition in which the gust separation is equal to eight times the gust length (note that the length of a single (1-cosine) gust is twice its gradient distance).

Results are shown in figure 3 for gust gradient distances from 10 m to 320 m. In figures 3(a), (b), and (c), results are shown respectively for 10 m and 20 m, 40 m and 80 m, and 160 m and 320 m. The lower limit of 10 m is constrained by the response times of the Gnat instrumentation system and the upper limit has been chosen to minimise effects of scale-length on the vertical component of turbulence, which is relatively small on account of ground proximity.

Figure 3(d) shows the results of averaging the measurements for the different gradient distances in pairs and also the combined overall average. The overall average is also shown in figure 12 (which is a less cluttered figure) where it is compared with an approximation based on linear-segments. The discussion of this averaged result is deferred to section 8.

It is apparent from figures 3(a), (b), and (c) that the measured values of P are significantly higher over the range of normalised displacements from 0 to 1 where the gust components overlap, than they are for values of normalised displacement greater than 1 where the gust components are sequential. In particular, in figure 3(c), which shows results for gradient distances of 160 m and 320 m, the values of amplitude-reduction factor when the normalised displacement is equal to 0 are greater than unity. As explained above, this condition corresponds to a 45-degree round-the-clock gust. Thus this particular result implies that, for the chosen 25 turbulence records, the average amplitude of the 45-degree gust was slightly greater (up to a factor of 1.2) than the average amplitude of the vertical and lateral gusts. It should be noted, however, that this conclusion is not applicable at the shorter gradient distances, figures 3(a) and (b), nor does it have a significant effect on the overall average result (figure 12). Our interpretation of the values of P greater than unity in this 45-degree round-the-clock condition is that, at the larger

gradient distances of 160 m and 320 m, the measured wind fluctuations reflect properties of the velocity vector directions in the airflow over underlying hilly terrain.

7.3 RESULTS FOR RANDOM-PHASE AND GAUSSIAN SIGNALS.

As a means of validating the principles underlying equation 20, it has been applied to two types of test signals.

First, for each of the Gnat runs used in the study, associated signals (corresponding to the vertical and lateral components) have been generated with random-phase. This process is described in appendix B. As the value of the amplitude-reduction factor of $P = 0.85$, proposed for use in a multiaxis gust requirement, is intended to represent the effects of phase correlation, section 4, this randomisation of phase should have a significant effect on the associated measured P values.

The results of this part of the study, in which randomised phase signals have been generated for each of the turbulence records used to produce the results in figure 3, are shown in figure 4. Figures 4(a) to 4(d) correspond to figures 3(a) to 3(d) respectively. In all of these cases the measured value of P for the signals with randomised phase is of order unity over the entire range of normalised displacements. Thus, it has been demonstrated that the departures in the values of P from the value of unity, measured using the Gnat turbulence data and illustrated in figure 3, are indeed associated with phase correlation.

Second, as a further example of a random phase signal, samples of a Gaussian random process have been generated in the form of Brownian noise (integral of a sequence of independent Gaussian random variables with zero mean), for which, in combination with the detection filters employed, equation 20 should give the theoretical result $P = 1$. The numbers of data points were chosen to correspond exactly to those in the Gnat turbulence records. The results, derived exactly as for the results in figures 4(a) to 4(d), are shown in figures 5(a) to 5(d). Again it can be seen that the theoretical result of $P = 1$ is recovered very closely. Thus confirming that the departures in the values of P from the value of unity, measured using the Gnat turbulence data and illustrated in figure 3, are associated with phase correlation.

7.4 MULTIAXIS COMPONENTS WITH DIFFERING GRADIENT DISTANCES.

Measurements of the amplitude-reduction factor P have also been made for multiaxis gust patterns comprising a pair of gust components, one in each of the vertical and lateral axes, having different gradient distances $H1$ and $H2$. Typical situations are illustrated in figures 6(a) and (b). As shown, the gust lengths AB and CD are equal to $2H1$ and $2H2$ respectively. As in figure 2, we introduce the terminology gust separation and gust displacement such that the gust displacement is the distance AC between the positions of onset of the respective gusts and the gust separation, which is negative when the gust components overlap, is the distance BC between the end of the first gust and the onset of the second gust. The condition illustrated in figure 6(a) is that of sequential, non-overlapping, gust components and that in figure 6(b) shows a case of complete overlap.

Following the method used to produce the results in figure 3, based on averages over 25 turbulence-velocity records, measured values of the amplitude-reduction factor P for pairs of gust components are presented in figures 7 to 11.

Figure 7(a) shows results for a filter pair V-VL (as described in section 7.1) in which the vertical gust component of the pair has a gradient distance of $H1 = 80\ m$ and the lateral component takes values for its gradient distance $H2$ of 80 m (duplicating results for components of equal gradient distance already described in section 7.2), 40 m, 20 m, and 10 m. Figure 7(b) shows analogous results for a filter pair L-LV in which the lateral gust component of the pair has a gradient distance of $H1 = 80\ m$ and the vertical component takes values for its gradient distance $H2$ of 80 m, 40 m, 20 m, and 10 m. In all cases the measured values of P are plotted as a function of the gust displacement AC, figure 6, normalised by the length $2H1$ of the longer gust. Averages of the results presented in figures 7(a) and (b) are shown in figure 8.

Analogous results for the situation in which the gradient distance of the longer gust component of the pair has a gradient distance of $H1 = 160\ m$ and the other component takes gradient distances of 160 m, 80 m, 40 m, and 20 m are shown in figures 9 and 10. The overall average from the results in figures 8 and 10 is shown in figure 11. The overall average is also shown in figure 13 where it is compared with an approximation based on linear segments. The discussion of this averaged result is deferred to section 8.

As for the measurements described in section 7.2, a value of the normalised displacement equal to unity again corresponds to the situation in which the onset of the second, shorter, gust component occurs at the endpoint of the longer gust, i.e., zero separation. However, as the vertical and lateral gust components are now generally different lengths, a value of the normalised displacement of zero no longer corresponds to a round-the-clock gust.

In the individual cases in which the ratio between the component lengths $H2/H1$ takes its minimum value of 1/8, it is meaningful again, as for sequential gust components, to conceptualise the pattern as two distinct gusts, in this case a long gust combined with a short gust, rather than as some complex three-dimensional structure of which the (1-cosine) components in the two axes are simply projections. In this situation a value of P of approximately 0.85 is again to be expected. Inspection of figures 7 and 9 for this case (data points represented by diamonds) broadly confirms this prediction. The values of P greater than unity, which can be seen at a normalised displacement of zero in figure 9 for gust components of equal length (data points represented by squares), correspond to the round-the-clock situation already discussed in section 7.2.

It can be seen from the results shown in figures 8 and 10, and for the further overall results shown in figures 11 and 13, that the effect of averaging the results for gust components which start at the same point (normalised displacement = 0) but have different lengths is to reduce the amplitude-reduction factor P to a value less than unity (approximately 0.9, results represented by triangles).

8. DISCUSSION.

The statistical results summarised in figures 12 and 13 provide the basis for the main conclusion of this report which is that a value of the amplitude-reduction factor of $P = 0.85$ for multiaxis pairs of (1-cosine) gusts in sequence (i.e., positive gust separation or equivalently normalised gust displacement greater than unity) is supported for use in the proposed new multiaxis gust model, according to equation 3. In fact, as can be seen in figures 12 and 13, the measured average value of P shows some dependence on gust separation. Under the particular condition when the two gust components have the same gradient distance, figure 12, P takes a value close to 0.9 at zero separation (normalised displacement = 1) and tends at larger separations to a value close to 0.8. Taken as a single number to cover the entire range of (positive) separations examined for this case, figure 12, a value of P of 0.85 can be seen to be slightly conservative. In contrast, for the cases with significant gust-component overlap, i.e., normalised displacement increasing from 0 to 1, P lies in the range from 1 to 0.9. For subsequent reference, the measured values of P are compared in figure 12 with an approximation, comprising linear segments, which takes a value of 0.85 for normalised gust displacement greater than unity (positive separations) and takes the form of a linear interpolation between 1 and 0.85 for normalised gust displacements between 0 and 1.

Analogous results are shown in figure 13 for the more general situation including cases in which the two gust components have different gradient distances, the ratio between gradient distances covering the range between 1 and 1/8. A comparison of figure 13 with figure 12 shows that averaging across these ratios results in a significant decrease in the measured value of the amplitude-reduction factor P over the entire range of normalised displacements, the measured averaged values now always lying below the linear-segment approximation.

9. FORMULATION OF PROPOSED REQUIREMENT.

It follows from the above discussion that one possibility for a revised airworthiness rule, to take account of multiaxis gust patterns, would be to adopt the linear-segment approximation, figure 13. Although for particular tuned gust patterns, in which the gradient distances of the two gust components are equal and the normalised displacement is less than 3, the model would slightly underestimate the associated loads (as shown by figure 12). When averaged over all of the conditions considered in this study, the linear-segment approximation would result in conservative load estimates in the sense that the measured data generally support a smaller value for P, figure 13, which would result in further reductions in loads.

However, an alternative and essentially equivalent rule, which would be rather simpler to implement, is illustrated in figure 14. For values of the normalised displacement > 1, P takes the value of 0.85 as in the linear-segment approximation. For values of the normalised displacement between 0 and 1, however, the linear-segment approximation (diagonal line in figure 14) is replaced by a continuation of the value $P = 0.85$ (dashed line in figure 14) combined with a round-the-clock single-gust analysis. As previously explained, the round-the-clock condition is equivalent to a pair of (1-cosine) gust components having equal length and zero displacement. This corresponds to the single point, designated by a circle in figure 14, on the linear-segment approximation where the normalised displacement = 0. By incorporating the round-the-clock

analysis as part of the proposed rule, figure 14, the region of the linear-segment approximation in the vicinity of normalised displacement = 0 would in effect be covered.

Cases in which the normalised displacement takes values within the interior of the region from 0 to 1 fall into two classes: those for which the two gust components have lengths of the same order and those for which a long gust component is combined with a short gust component. The former cases are effectively covered by the round-the-clock condition, corresponding to the circle in figure 14, the fact that this condition is not exactly the tuned condition being compensated by its being applied with P = 1, rather than with a value P < 1 as allowed by the linear-segment approximation within the range of normalised displacements from 0 to 1, figure 14. The second class, comprising cases in which a long gust component is combined with a short gust component, has been discussed in section 7.4, where it was shown that the measurements support the use of an amplitude-reduction factor of $P = 0.85$. These cases are thus covered by the dashed line extension of the line $P = 0.85$ illustrated in figure 14.

10. APPLICATION TO ENGINE NACELLE RESPONSES OF AIRBUS-TYPE MATHEMATICAL MODEL.

Based on an Airbus-type aircraft dynamical model, used in a previous study for the FAA, a comparison is made in table 1 between the loads resulting from the proposed multiaxis model and those from an isolated tuned-discrete-gust in a single axis, as in the current requirement. Results are given for eight load quantities, which include accelerations, forces, and moments:

1. I/B_ENG_Y-ACCN
2. I/B_ENG_Z-ACCN
3. I/B_ENG_FX
4. I/B_ENG_FY
5. I/B_ENG_FZ
6. I/B_ENG_MX
7. I/B_ENG_MY
8. I/B_ENG_MZ

and for two flight cases: Flight Case 1: sea level, *Vc Mach=0.499*, high weight, *Vtas=169.8 m/s* and Flight Case 2: 25000 ft, *Vc Mach=0.76*, low weight, *Vtas=237 m/s*.

In table 1, following the notation introduced in section 1, the first column gives the load x_1 due to a tuned isolated gust in the vertical axis and the second column gives the load x_2 due to a tuned isolated gust in the lateral axis. Column three gives the result of combining these loads according to equation 2. The fourth column is the predicted multiaxis load, obtained by multiplying the magnitudes in the third column by the amplitude-reduction factor P, with numerical value $P = 0.85$.

Comparing the resulting multiaxis loads with those from an isolated discrete gust analysis, in both the vertical and lateral axes, it can be seen that in most of the cases considered the multiaxis load is larger than either of the corresponding single-axis loads. However, this is not always the case. Specifically, in Flight Case 1 a single-axis load is the design case for load quantities 4 and 7, and in Flight Case 2 the same is true for load quantities 1, 3, 4, and 7. It should be noted that

it is only through the introduction of an amplitude-reduction factor P with magnitude less than one that the single-axis load sometimes dominates. The magnitudes in column three of table 1, which exclude this factor, can never be less than the greater of the single-axis loads in the first two columns. This is consistent with a principle first introduced in the SDG1 method [3,4] where it is through analogous energy-reduction factors that loads associated with a simple pattern (few ramp components), in many cases, exceed those associated with a more complex pattern.

A similar comparison is made in table 2 between between the loads resulting from the proposed multiaxis model (second column) and those from a round-the-clock tuned-discrete gust analysis (first column). It can be seen that the multiaxis load is greater than the round-the-clock load in 7 of the 16 conditions considered. Again, it is the introduction of the amplitude-reduction factor which allows the round-the-clock load sometimes to be the greater of the two; without this factor the multiaxis load would always be an upper bound to the round-the-clock load.

Comparisons are made in table 3 between the multiaxis method proposed in this report, based on a tuned (1-cosine) gust component in each axis, and the PSD (power-spectral-density) multiaxis method (PSDMA). Results are expressed as percentage increases in load in going from the associated worst-case single-axis response to the multiaxis response (i.e. the PSDMA result is compared with the worst-case single-axis PSD load). Percentage increases in load in going from the worst-case, single-axis isolated discrete gust (IDG) to an isolated discrete gust round-the-clock (IDGRC) are also shown.

The results presented in table 3, column two, indicate that, in isolation, the round-the-clock IDG method is insufficiently representative of multiaxis loads in that it is too sensitive to the constraint that large responses in the vertical and lateral axes occur not only for the same gust gradient distance but also that the associated response time histories peak at the same instant. However, it can be seen to be complementary to the proposed multiaxis method based on independently tuned (1-cosine) gust components in each axis, time phased to give their peak loads at the same instant. Taken together, columns two and three of table 3, the two methods predict more representative load increases in going from a single-axis to a multiaxis analysis.

Because of the introduction of the amplitude-reduction factor (proposed value $P = 0.85$), the load increase introduced by the proposed multiaxis method can never exceed a maximum value of approximately 20%, a value seen to be exceeded in several instances by the multiaxis PSD analysis (first column of table 3).

11. PREDICTED LOADS COMPARED WITH LOADS RESULTING FROM MEASURED TURBULENCE INPUTS.

In the following, a statistical analysis is presented of the engine nacelle loads resulting when the aircraft dynamic model used in section 10 is subjected to simultaneous measured turbulence inputs in the vertical and lateral axes. The measured data are from the gust measurement programme described in section 5.3 and form a subset of ten turbulence-velocity time histories of the set of 25 used in section 7 to derive a value for the amplitude-reduction factor P. The ten runs have been selected as those most representative of isotropic turbulence, the gusts in the vertical and lateral axes being on average of approximately the same amplitude.

Time histories of response have been computed for all eight of the load quantities listed in section 10 and for each of the two flight cases, even though Flight Case 2 refers to response at 25000 ft. and the turbulence records were all measured below 1000 ft. The justification in this latter case is that the following analysis makes no reference to the absolute amplitudes of the loads but only to their relative magnitudes. Thus, for the results to be meaningful, it is required only the the *shapes* of the turbulence fluctuations be sufficiently representative, and this is assumed to be the case.

The statistical analysis of the engine nacelle loads is similar to the method of statistical analysis of turbulence records described in section 6. For each of the load quantities and flight cases, local maxima and minima in the response time histories are identified and cumulative distributions of their magnitudes are derived. The results, presented in figures 15 and 16, have been produced using a general-purpose analysis program for normalising log-linear plots of threshold-exceedance rates in which y is used to denote threshold amplitude and Ny is used to denote rate-of-exceedance (per unit distance in this case) of threshold y. Thus here we make the identification:

y : load amplitude
Ny : rate of occurrence of local maxima and minima of magnitude exceeding threshold y.

In figures 15 and 16, for Flight Cases 1 and 2 respectively, the above variables are normalised in the form $(y/Gn)^c$ and Ny/An, where the subscript n refers to the respective load quantity listed in section 10. In these figures, the normalising factor An and the exponent c are both taken to be unity. In figures 15a and 16a, the normalising factor Gn is also taken to be unity; thus these plots show the raw unnormalised exceedance rates. It should be noted that, because of the large disparity between the numerical magnitudes of the different load quantities, two of the plots lie effectively on the vertical axis.

In order to compare the measured loads with the predicted loads resulting from the proposed multiaxis analysis method, the normalising factor Gn is taken in figures 15b and 16b, for each load quantity n, to be the maximised response resulting from the procedure defined in section 1 and given by equation 2. This quantity is tabulated, for each load, in the third column of table 1. Note that this quantity does not include the amplitude-reduction factor P; however, as we shall be concerned only with the *ratios* of loads, such a constant factor does not affect our conclusions.

Consistency between the measured and predicted loads requires that the resulting normalised curves, figures 15b and 16b, be parallel. In a more complete theory, formulated for the purposes of a Mission Analysis, rather than a Design Envelope criterion, associated values for the normalising factor An, analogous to the n_0 term in a PSD Mission Analysis, would also be predicted. Consistency of this more complete prediction with the measured loads would then require that, using these An values to normalise the vertical axis, the normalised plots collapse to a single curve. However, as both the existing tuned-discrete-gust requirement and its multiaxis extension proposed here are Design Envelope requirements, for present purposes, it is sufficient to use normalising factors $An = 1$ and to require only that the normalised curves be parallel.

In figures 15b and 16b it can be seen that most of the normalised curves satisfy very well the requirement that they be parallel. There are, however, some exceptions. In Flight Case 1, figure 15b, load quantities 8 and 6 stand out in the sense that the predicted loads (represented by the *Gn* factors) are too low. The same is true of load quantity 8 in Flight Case 2, figure 16b. However, analogous results (not presented here) have also been obtained in a related study in which responses, due to measured lateral turbulence, have been compared with predicted loads obtained using the existing tuned-discrete-gust method in the lateral axis only. As in the multiaxis case described above, the response magnitudes of load quantities 6 and 8 were underestimated.

The reason for this disparity has been determined by applying the existing (single-axis) SDG1 method [3,4] to the responses of load quantities 1 to 8 with lateral gust inputs and also by applying a (recently developed) multiaxis extension of the SDG1 method with combined vertical and lateral gust inputs. From this supplementary study it has been determined that, in both flight cases, load quantities 6 and 8 have a (SDG) tuned response containing a significant low-frequency (Dutch Roll) component associated with lateral gusts having gradient distance of 2000 ft. The under-estimate of response magnitudes in load quantities 6 and 8, apparent in figures 15b and 16b, is thus associated with the fact that neither the existing isolated-tuned-gust requirement nor its proposed multiaxis extension is intended to represent gust inputs of such large gradient distance.

We conclude from the results of the present comparison of predicted loads with loads resulting from measured turbulence inputs, shown in figures 15 and 16, that whilst the proposed multiaxis extension of the existing tuned-discrete-gust method inherits from the tuned-discrete-gust requirement the limitation that it tends to underestimate loads associated with lateral gust inputs of very large gradient distance over the range of gradient distances that it is intended to cover, it leads to predicted multiaxis loads consistent with those resulting from measured turbulence.

12. CONCLUSIONS.

A proposed new method for multiaxis gust analysis has been described, section 1, in which the associated gust model incorporates a pair of vertical and lateral one-minus-cosine components. The theoretical basis for this method, which involves the application of equations 1 and 2, has been presented. The derivation of these formulas is based on the concept of generalised energy as a means of quantifying probability, section 2. In section 2.2 it has been shown how this concept can be generalised to the multiple-axis situation.

The introduction of a further amplitude-reduction factor P, to take account of phase correlations which are neglected in the derivation of equations 1 and 2, has been described. In reference 2 it was proposed that a value for this factor of $P = 0.85$ (equation 3) would be consistent with previous analysis of severe gusts encountered by civil aircraft during routine operational flying (the CAADRP programme). Whilst the CAADRP database only provides evidence for the effects of gusts in a single axis (the vertical), it does allow an estimate to be made of the relative effects of a single (1-cosine) gust in the vertical axis and of a sequence of two such gust components in the same axis. Reference 2 presents preliminary evidence that the same value of P is applicable in the multiaxis situation.

To further justify the use of the factor $P = 0.85$ in the multiple-axis situation in which a (1-cosine) gust component occurs in each axis, evidence has been presented from a database of turbulence measurements made using a specially instrumented Gnat two-seat trainer aircraft. These measurements include simultaneous recordings of the vertical and lateral components. Particular runs from this database have been selected as having similar characteristics, in terms of intermittency and intensity, to those which have previously been associated with large excursions in aircraft normal acceleration during routine operational flying. Typical examples are illustrated in figure 1.

A method of data analysis has been described in section 6.2 in which the value of P is derived from the slopes of measured statistical distributions which correspond respectively to the occurrence of single (1-cosine) gusts and of pairs of (1-cosine) gusts, one in each of the vertical and lateral axes. The application of this method is illustrated by examples in appendix A.

Overall results of these measurements are summarised in figures 12 and 13. Figures 12 and 13 also illustrate a linear-segment approximation which for the overall averaged results (figure 13, which includes cases in which the two gust components have different gradient distances) provides an upper bound to the measured values of P.

This linear-segment approximation could be used as the basis of an airworthiness requirement to cover multiaxis gust encounters. However, in section 9 the case has been presented for an alternative and essentially equivalent rule, illustrated in figure 14, which would be rather simpler to implement. This rule requires the application of the multiaxis model, as described in section 1, incorporating an amplitude-reduction factor P of 0.85, equation 3, irrespective of gust displacement, but also requires that this multiaxis gust analysis be combined with a round-the-clock single-gust analysis for which $P = 1$.

The results of applying both the proposed multiaxis gust model and a round-the-clock analysis to engine nacelle responses of an Airbus-type mathematical model have been described in section 10. These results indicate that, in isolation, the round-the-clock method is insufficiently representative of multiaxis loads in that it is too sensitive to the constraint that large responses in the vertical and lateral axes occur not only for the same gust gradient distance but also that the associated response time histories peak at the same instant. However, it is shown to be complementary to the proposed multiaxis method based on independently tuned (1-cosine) gust components in each axis. Taken together, the two methods are shown to predict more representative load increases in going from a single-axis to a multiaxis analysis.

Finally, a comparison has been made, in section 11, using the same mathematical model of Airbus-type engine nacelle responses between loads predicted by the proposed multiaxis method and calculated loads resulting from measured simultaneous turbulence inputs in the vertical and lateral axes. It has been concluded that, whilst the proposed multiaxis extension inherits from the existing tuned-discrete-gust requirement the limitation that it tends to underestimate loads associated with lateral gust inputs of very large gradient distance, over the restricted range of gradient distances that it is intended to cover it leads to predicted multiaxis loads consistent with those resulting from measured turbulence.

13. REFERENCES.

1. J.G. Jones. Gust Analysis Method Incorporating a Multiaxis Pair of Vertical and Lateral One-Minus-Cosine Gusts. Gust Specialists Meeting, Montreal, Canada, July 7, 1998.

2. J.G. Jones. Theoretical and Empirical Basis for a Multiaxis One-Minus-Cosine Gust Model. Gust Specialists Meeting, Montreal, Canada, July 7, 1998.

3. J.G. Jones and G.H. Watson. Algorithms for Linear SDG Analysis. Stirling Dynamics Ltd. Report No. Report No. SDL-231-TR-2, Issue 2, June 1996.

4. J.G. Jones and G.H.Watson. Demonstration of Linear SDG Analysis. Stirling Dynamics Ltd. Report No. SDL-231-TR-3, Issue 2, June 1996.

5. J.G. Jones. Response of Linear Systems to Gaussian Process Inputs in Terms of Probability Functionals. Royal Aircraft Establishment (UK) Technical Report 86028, 1986.

6. J.G. Jones. On the Implementation of Power-Spectral Procedures by the Method of Equivalent Deterministic Variables, Part 2, Discrete-Element Technique. Royal Aircraft Establishment (UK) Technical Memorandum, Space 335, 1984.

7. V. Card. Computer Simulation Studies of the Statistical Discrete Gust Method. A compilation by Stirling Dynamics Ltd. from unpublished internal British Aerospace reports issued during the period 1978 to 1980. Stirling Dynamics Ltd., Report Number SDL-231-TR-4, 1996.

8. J.G. Jones and M. King. SDG Analysis of Turbulence Data for Aircraft Structural Design Requirements. SD-Scicon, Contract Report C26611/R-01/2, October 1991.

9. J.G. Jones. Statistical Discrete Gust Method for Predicting Aircraft Loads and Dynamic Response. Journal of Aircraft, Vol. 26, No. 4, 1989, pp. 382-392.

10. J.G. Jones. The Statistical Discrete Gust (SDG) Method in its Developed Form. 30th AIAA/ASME/AHS/ASCE Structures, Structural Dynamics and Materials Conference, Mobile, Alabama, 1989.

11. G.W. Foster and J.G. Jones. Analysis of Atmospheric Turbulence Measurements by Spectral and Discrete-Gust Methods. Aeronautical Journal, Vol. 93, p. 162, 1989.

12. J.G. Jones, G.W. Foster, and P.G. Earwicker. Wavelet Analysis of Gust Structure in Measured Atmospheric Turbulence Data, Journal of Aircraft, Vol. 30, No. 1, p. 94, 1993.

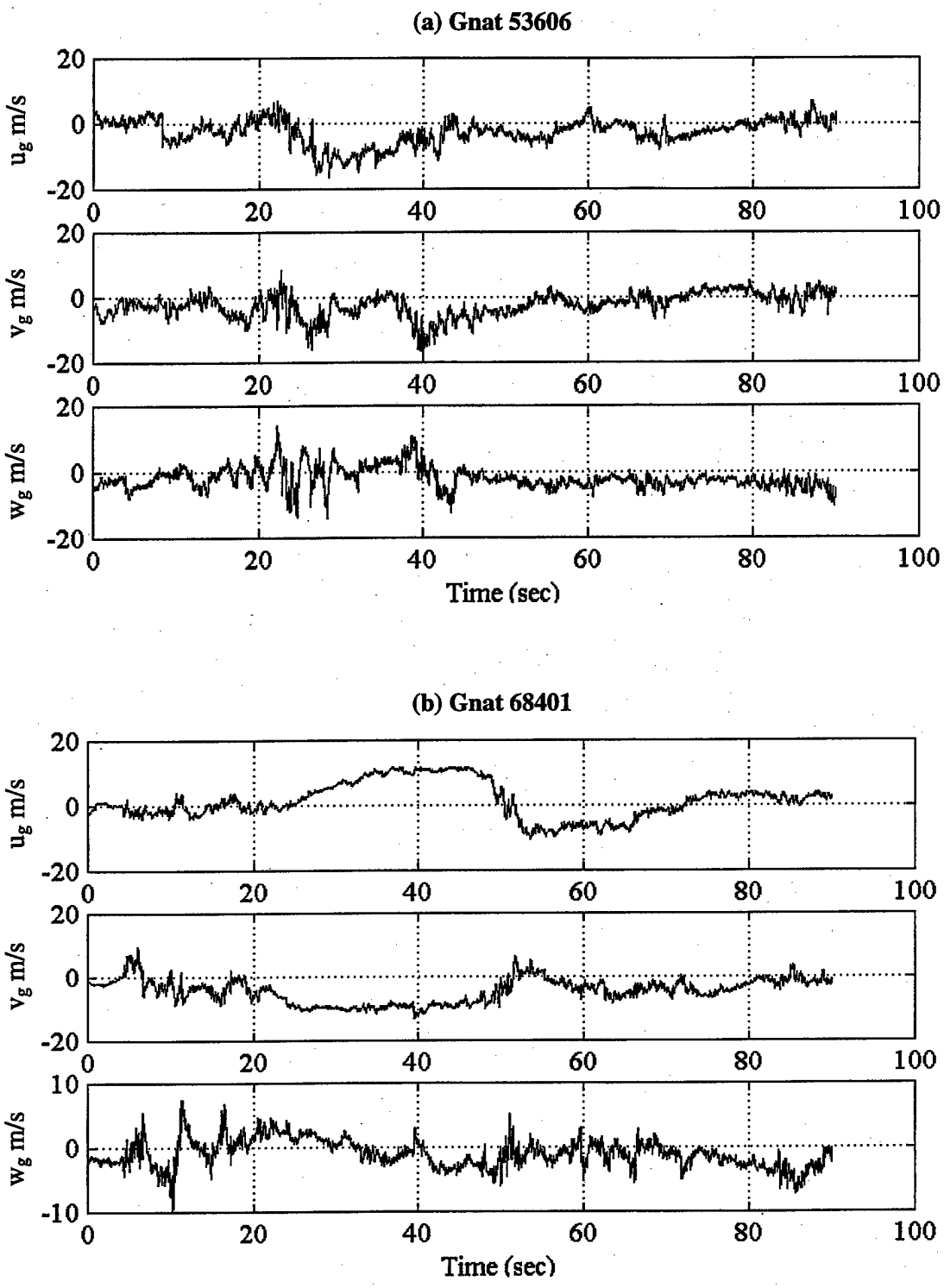

FIGURE 1. EXAMPLES OF THREE COMPONENTS OF TURBULENCE: u_g (HORIZONTAL), v_g (LATERAL), AND w_g (VERTICAL) MEASURED BY GNAT AIRCRAFT

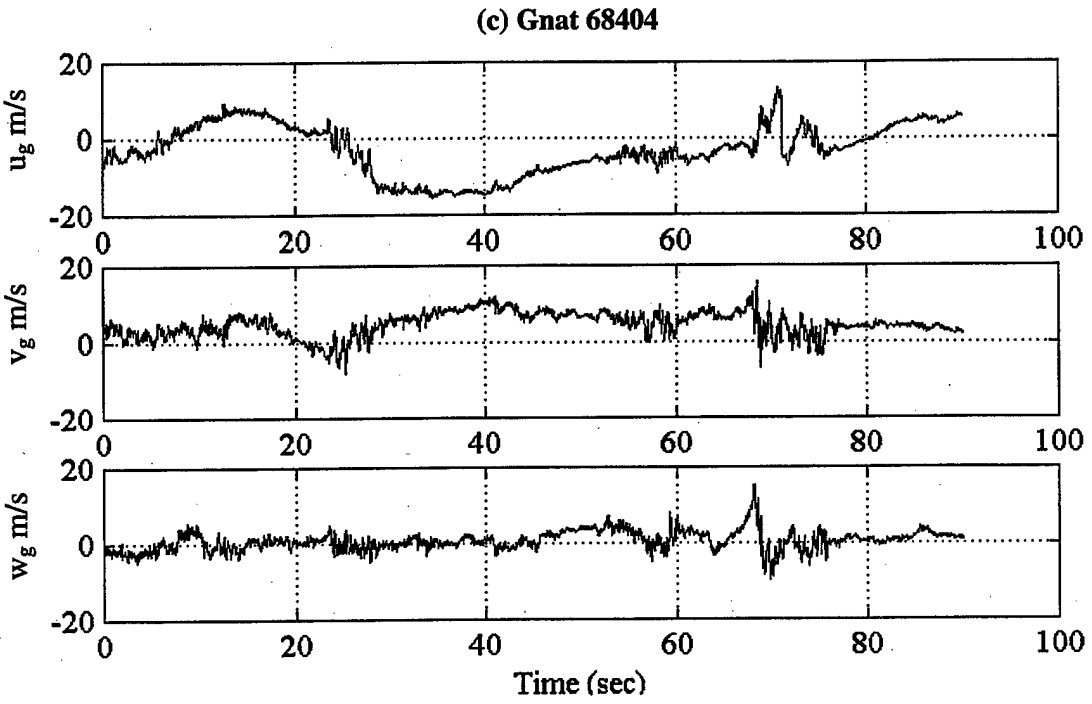

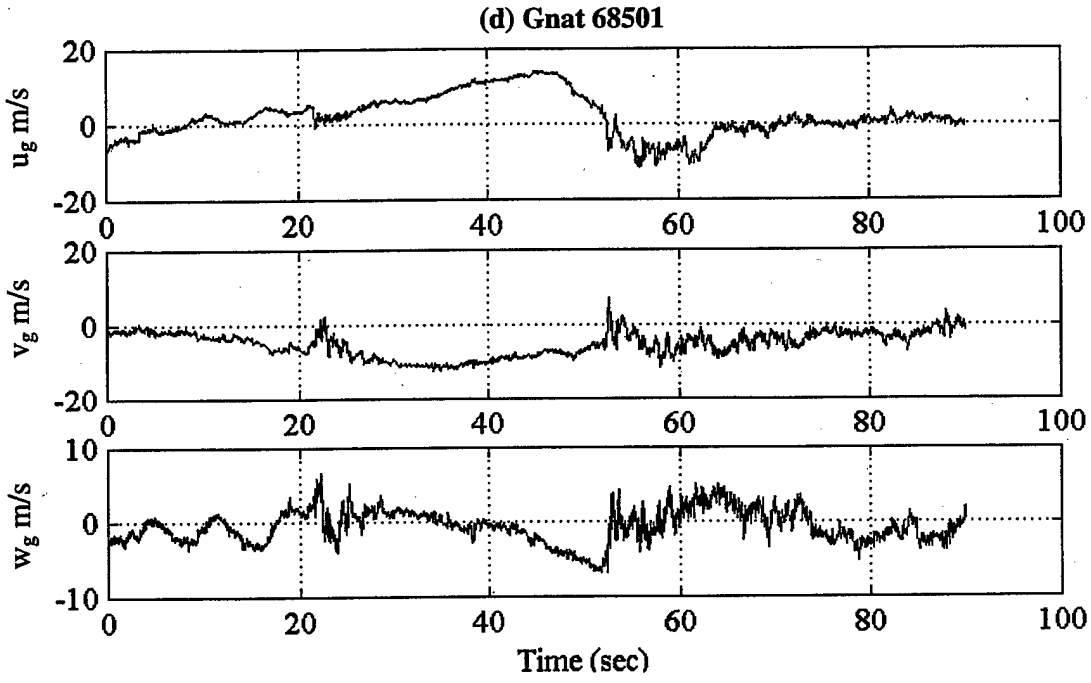

FIGURE 1. EXAMPLES OF THREE COMPONENTS OF TURBULENCE: u_g (HORIZONTAL), v_g (LATERAL), AND w_g (VERTICAL) MEASURED BY GNAT AIRCRAFT (Continued)

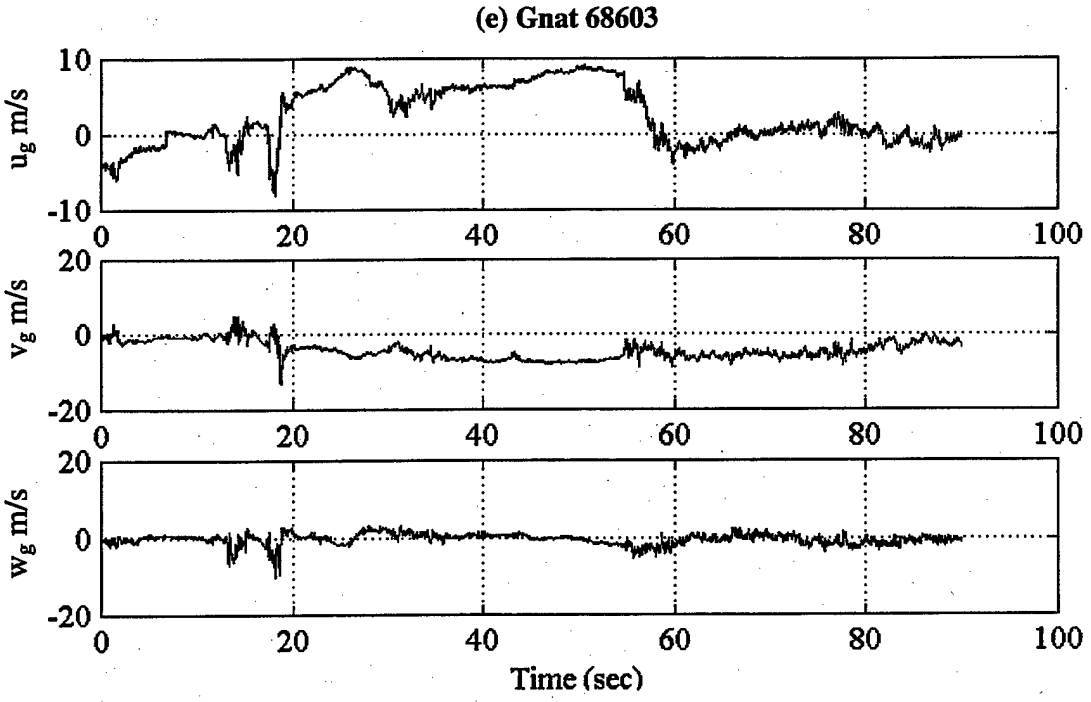

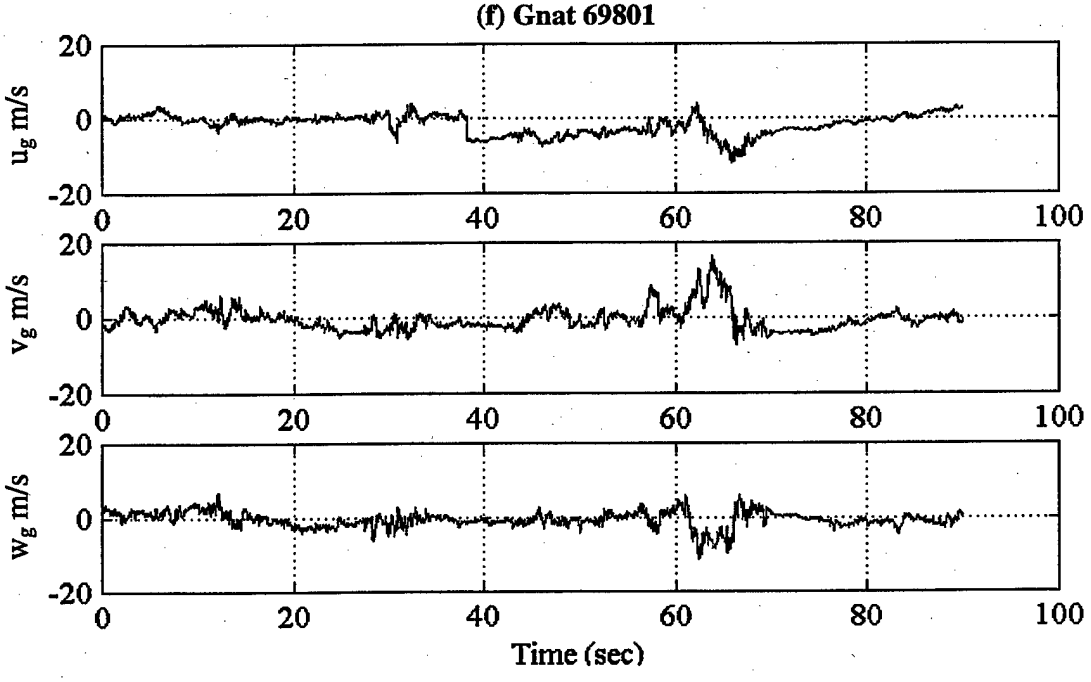

FIGURE 1. EXAMPLES OF THREE COMPONENTS OF TURBULENCE: u_g (HORIZONTAL), v_g (LATERAL), AND w_g (VERTICAL) MEASURED BY GNAT AIRCRAFT (Continued)

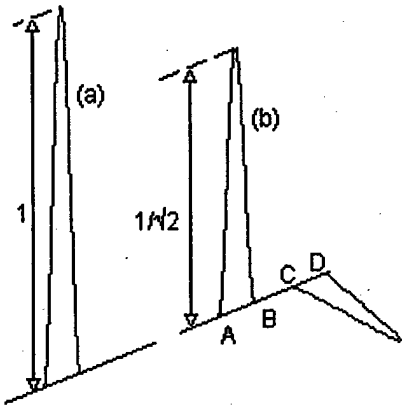

AB = CD = 2H
BC = gust separation
AC = gust displacement = 2H + BC

where,
H - Gradient distance

FIGURE 2. (a) SINGLE (1-COSINE) GUST AND (b) MULTIAXIS GUST PAIR SCALED IN AMPLITUDE TO HAVE EQUAL GENERALISED ENERGY AND HENCE EQUAL PROBABILITY

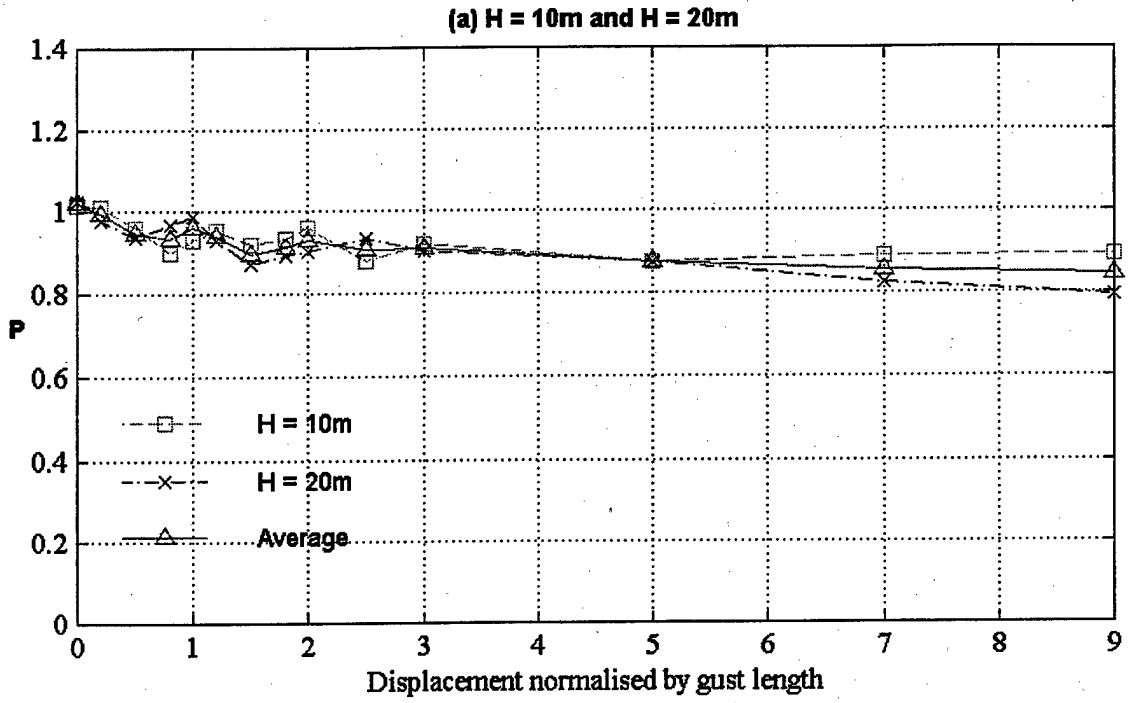

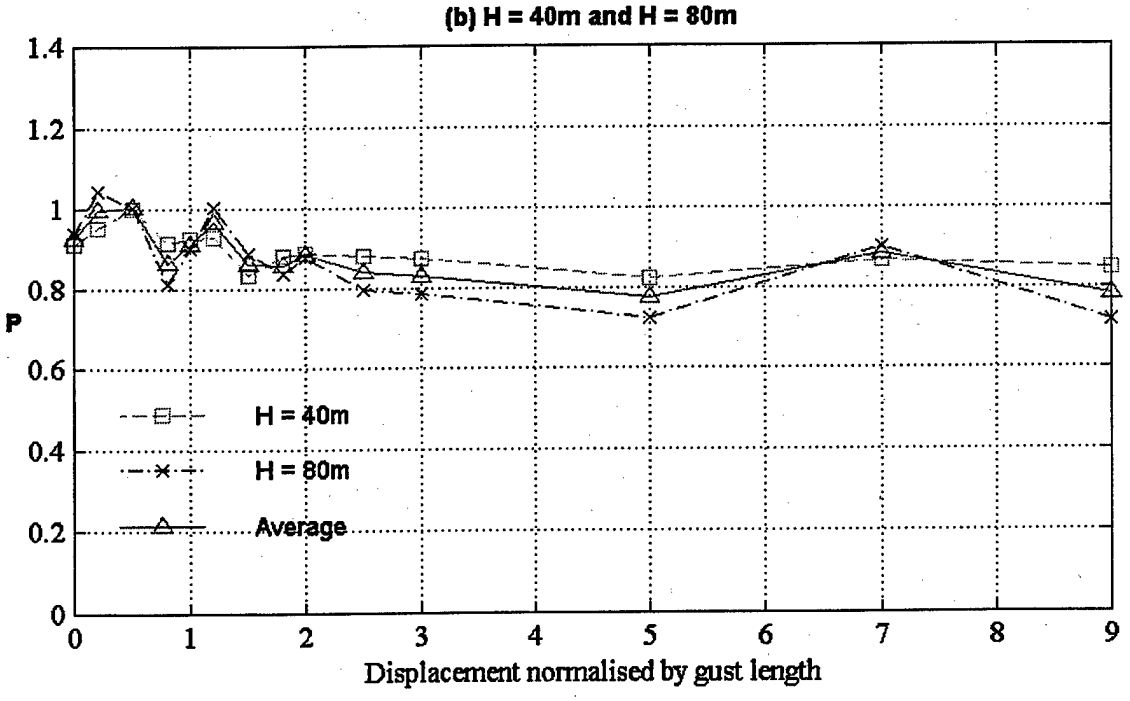

FIGURE 3. MEASURED VALUE OF AMPLITUDE-REDUCTION FACTOR *P* AVERAGED OVER 25 RUNS FOR GUST COMPONENTS HAVING SAME GRADIENT DISTANCE H

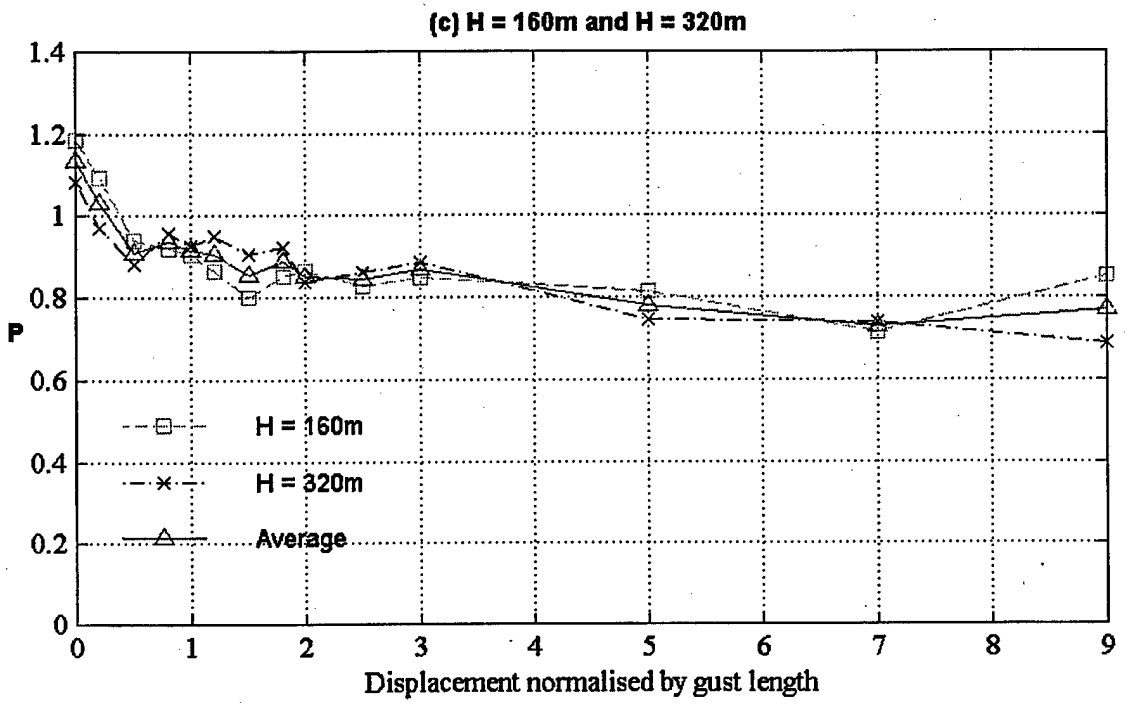

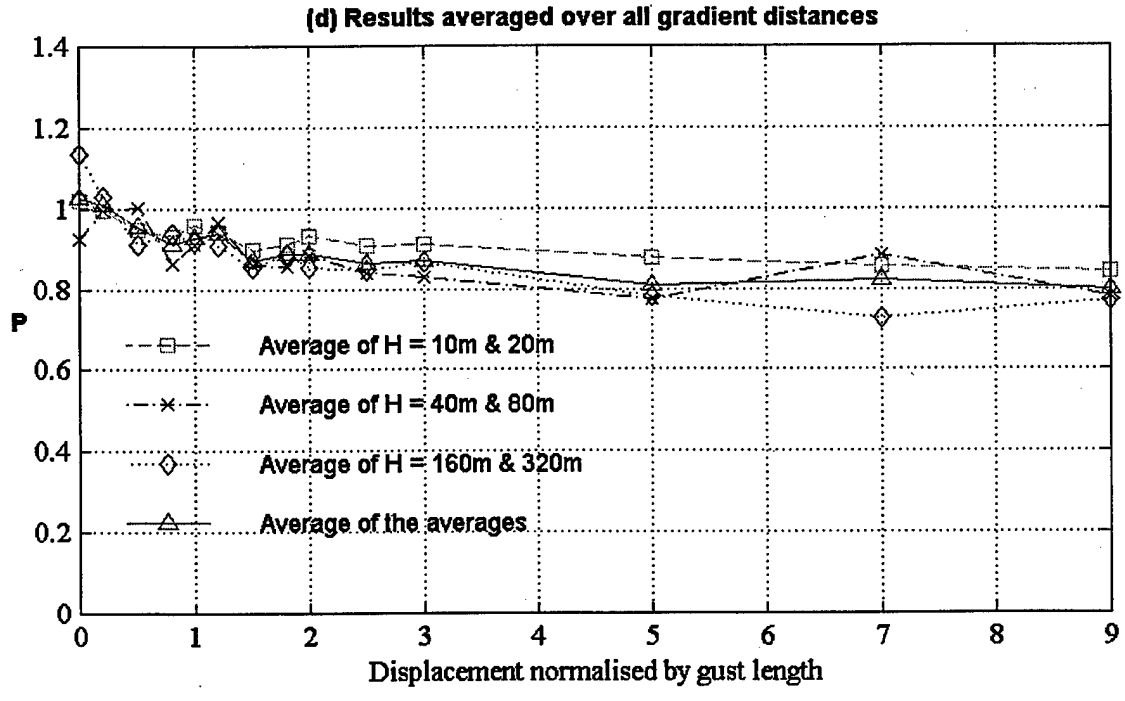

FIGURE 3. MEASURED VALUE OF AMPLITUDE-REDUCTION FACTOR *P* AVERAGED OVER 25 RUNS FOR GUST COMPONENTS HAVING SAME GRADIENT DISTANCE H (Continued)

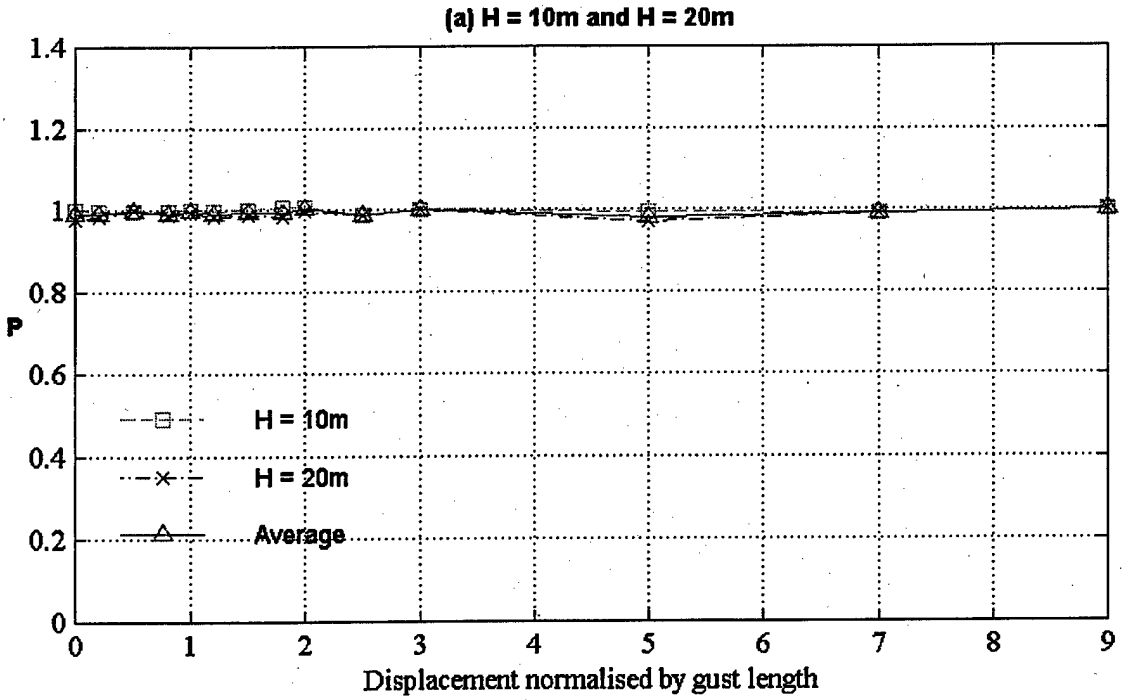

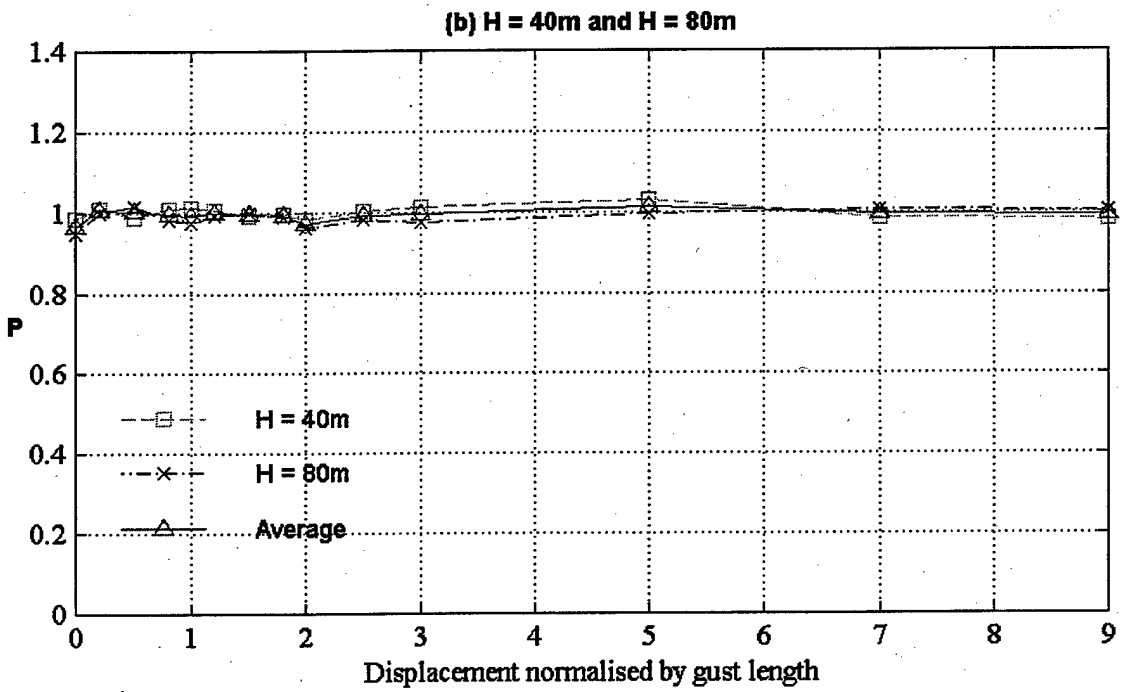

FIGURE 4. MEASURED VALUE OF AMPLITUDE-REDUCTION FACTOR *P* AVERAGED FOR SAME DATA AS IN FIGURE 3 BUT WITH RANDOMISED PHASE

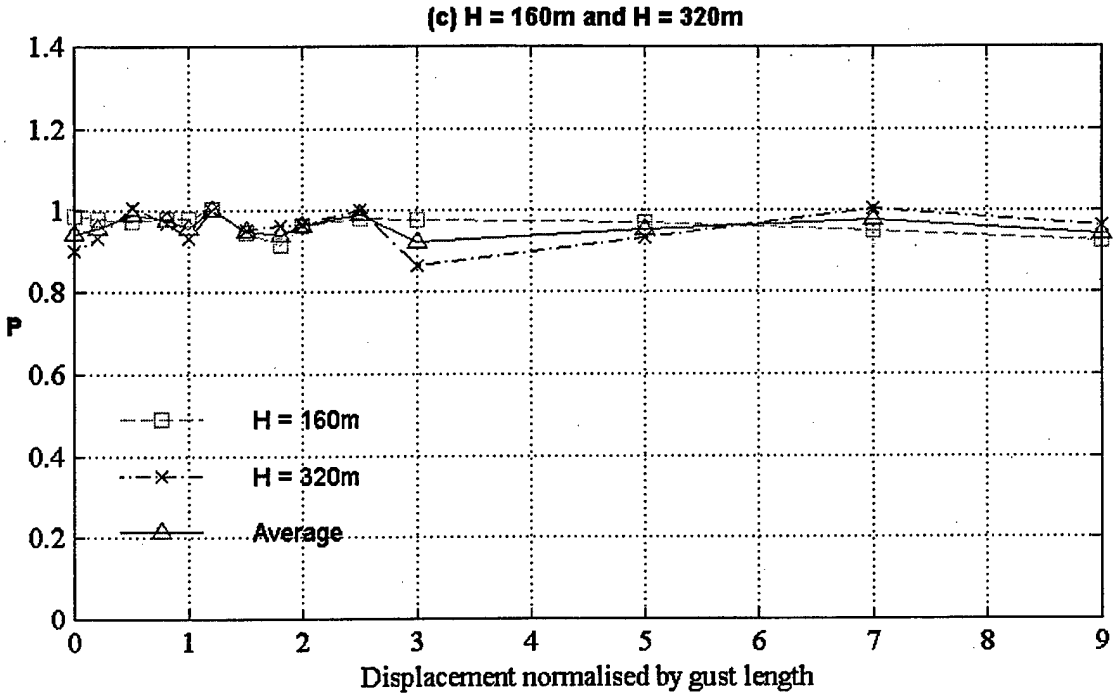

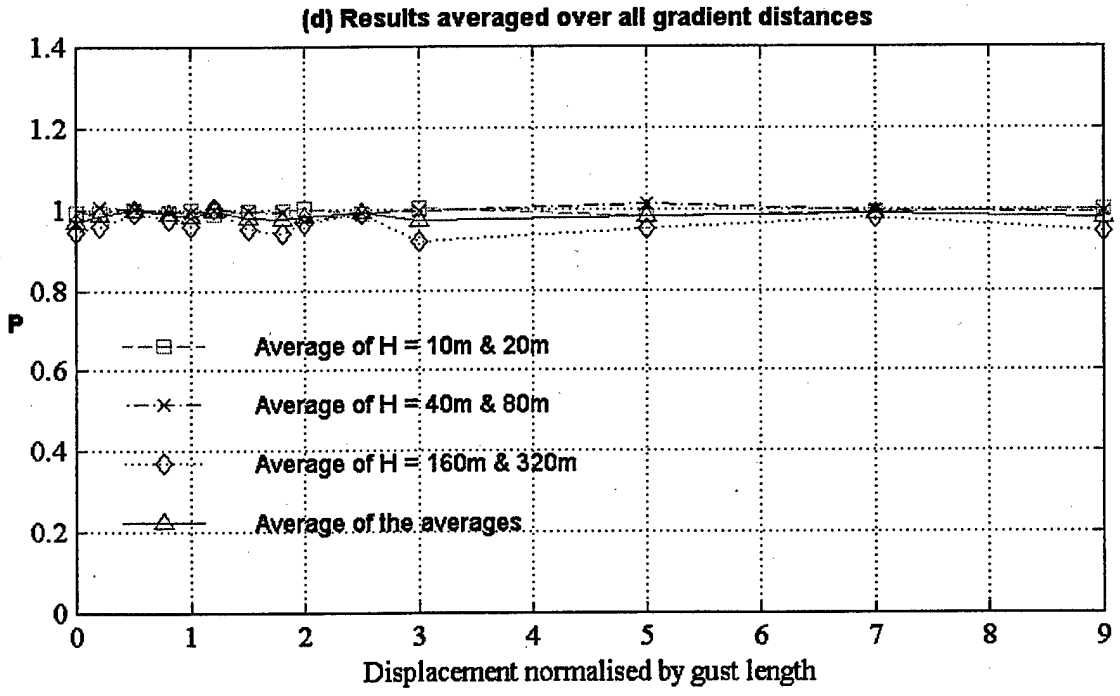

FIGURE 4. MEASURED VALUE OF AMPLITUDE-REDUCTION FACTOR *P* AVERAGED FOR SAME DATA AS IN FIGURE 3 BUT WITH RANDOMISED PHASE (Continued)

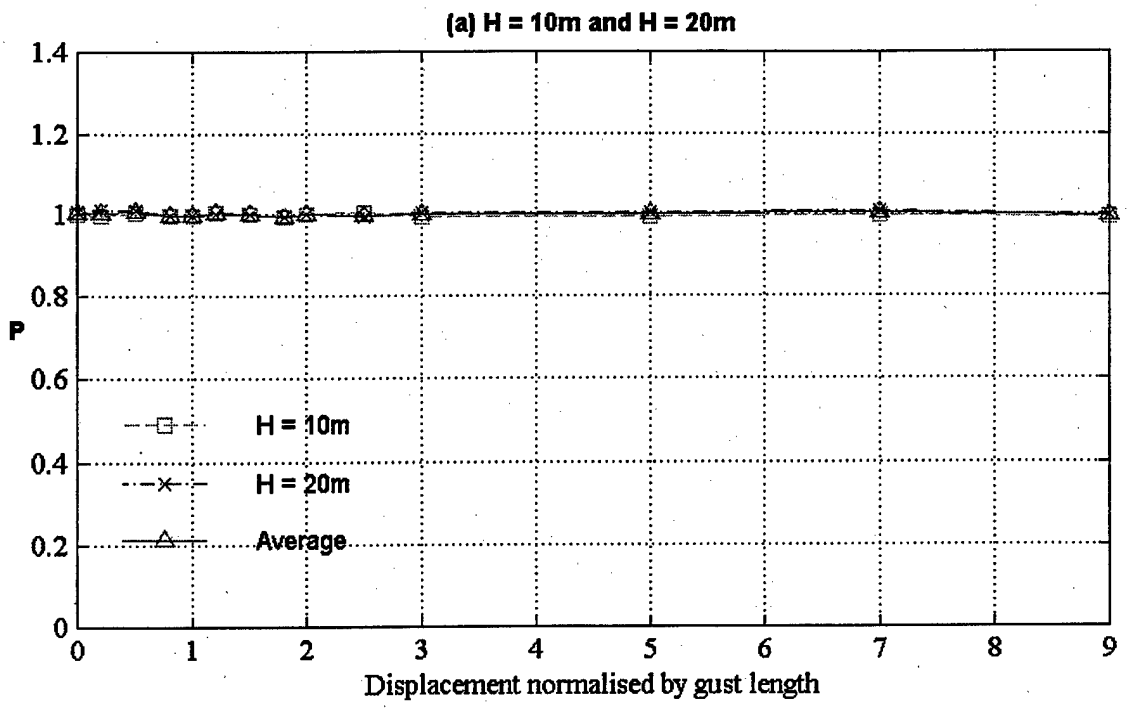

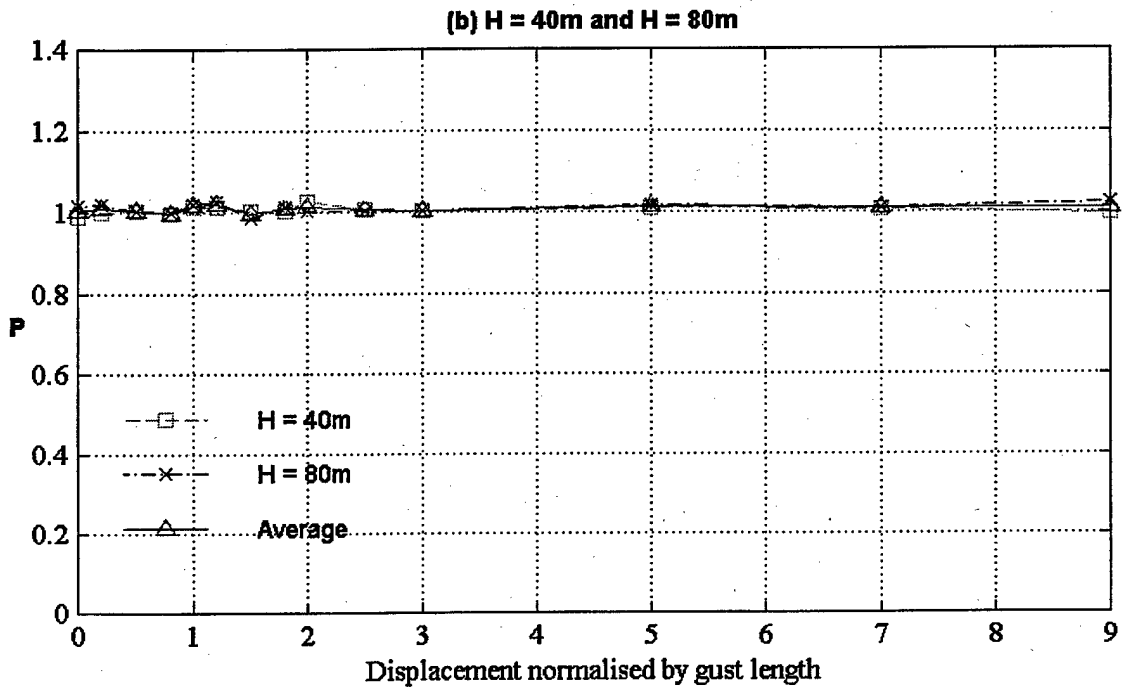

FIGURE 5. MEASURED AVERAGE VALUE OF AMPLITUDE-REDUCTION FACTOR *P* FOR GAUSSIAN SIGNALS HAVING SAME TOTAL LENGTH AS MEASURED TURBULENCE RECORDS

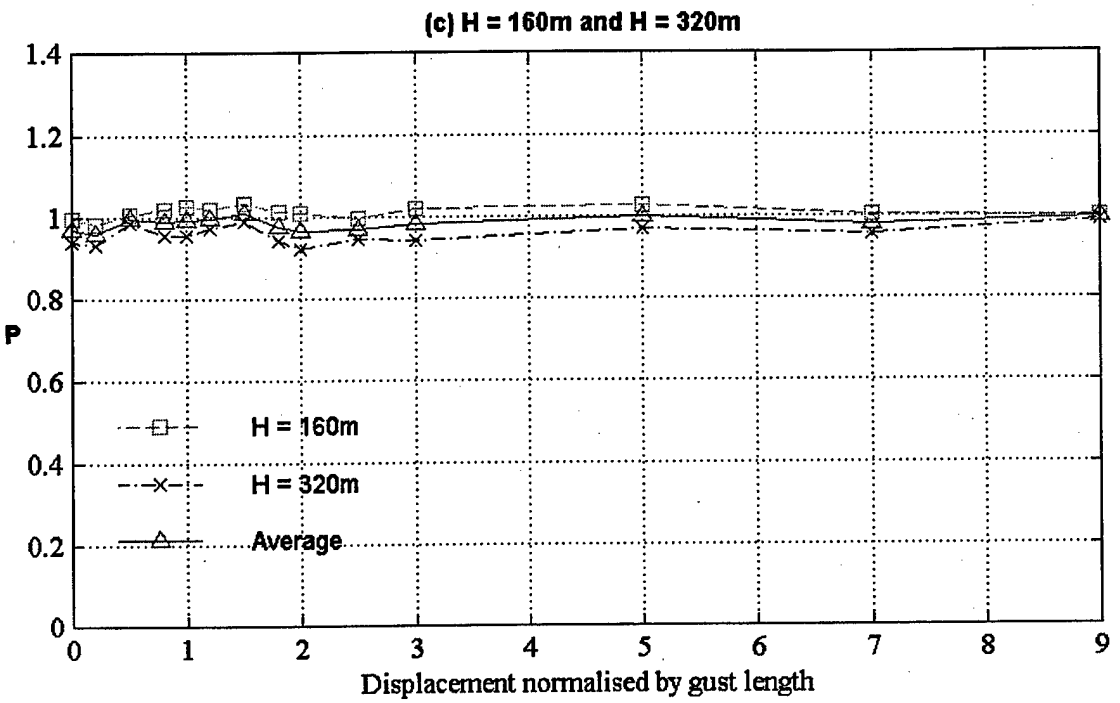

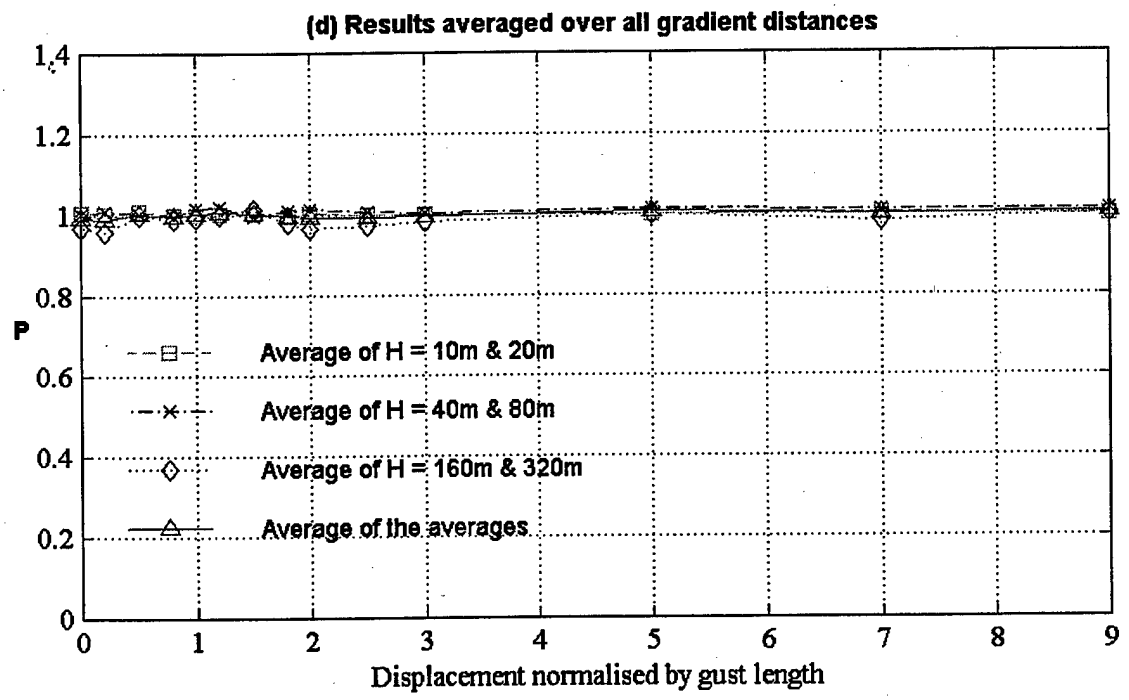

FIGURE 5. MEASURED AVERAGE VALUE OF AMPLITUDE-REDUCTION FACTOR *P* FOR GAUSSIAN SIGNALS HAVING SAME TOTAL LENGTH AS MEASURED TURBULENCE RECORDS (Continued)

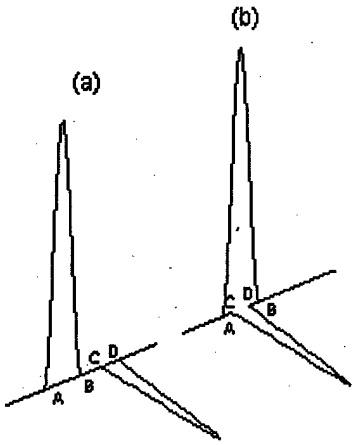

AB = 2H1
CD = 2H2
BC = gust separation (can be –ve)
AC = gust displacement = 2H1 + BC

where,

H1 - gradient distance of longer gust
H2 - gradient distance of shorter gust

(a) Sequential non-overlapping gust components
(b) Vertical gust component completely overlapping lateral gust component

FIGURE 6. MULTIAXIS GUST PAIR (VL) COMPRISING GUST COMPONENTS HAVING DIFFERENT GRADIENT DISTANCES

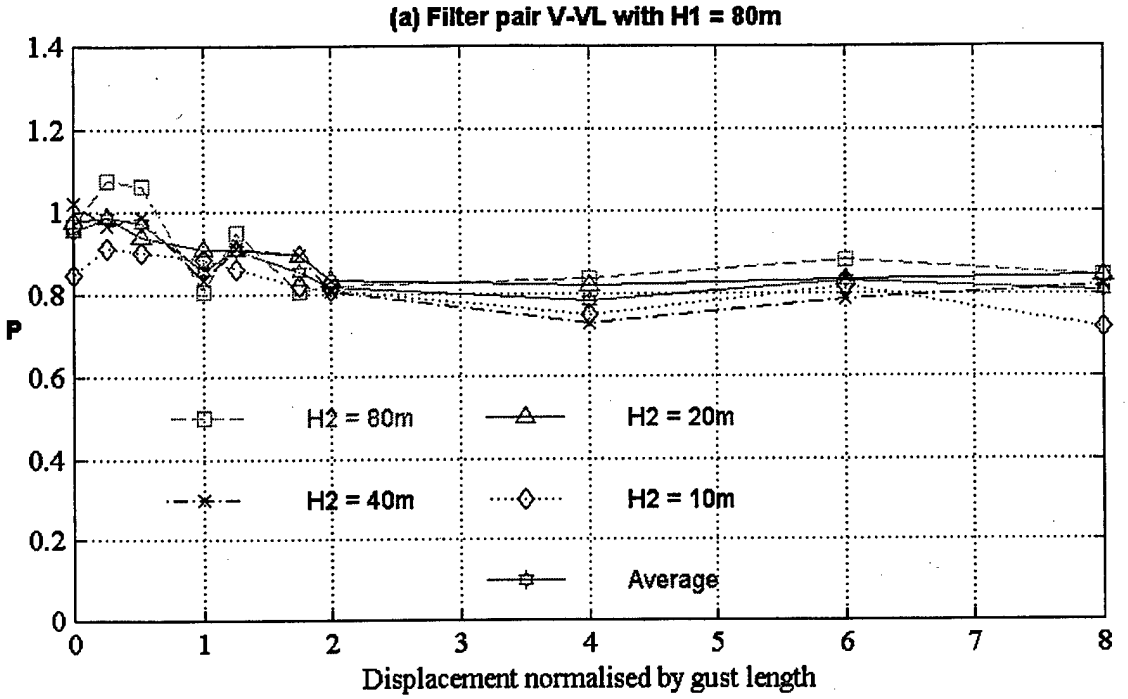

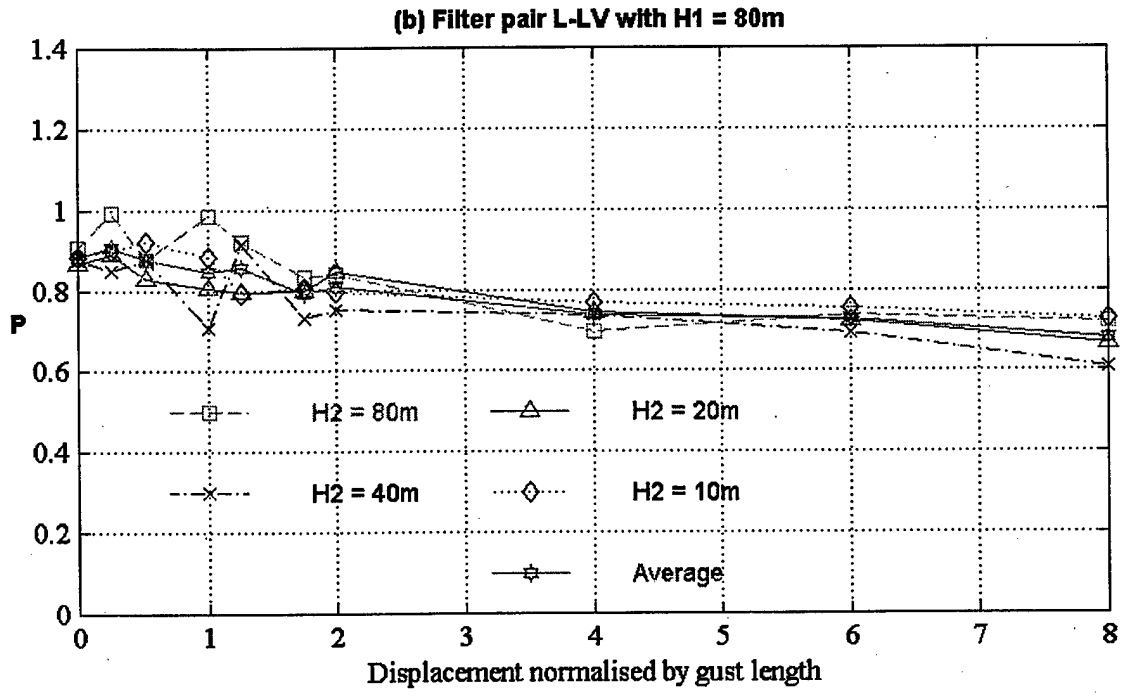

FIGURE 7. MEASURED VALUE OF AMPLITUDE-REDUCTION FACTOR *P*, AVERAGED OVER 25 RUNS, INCLUDING GUST COMPONENTS HAVING DIFFERENT GRADIENT DISTANCES, H1 = 80 m

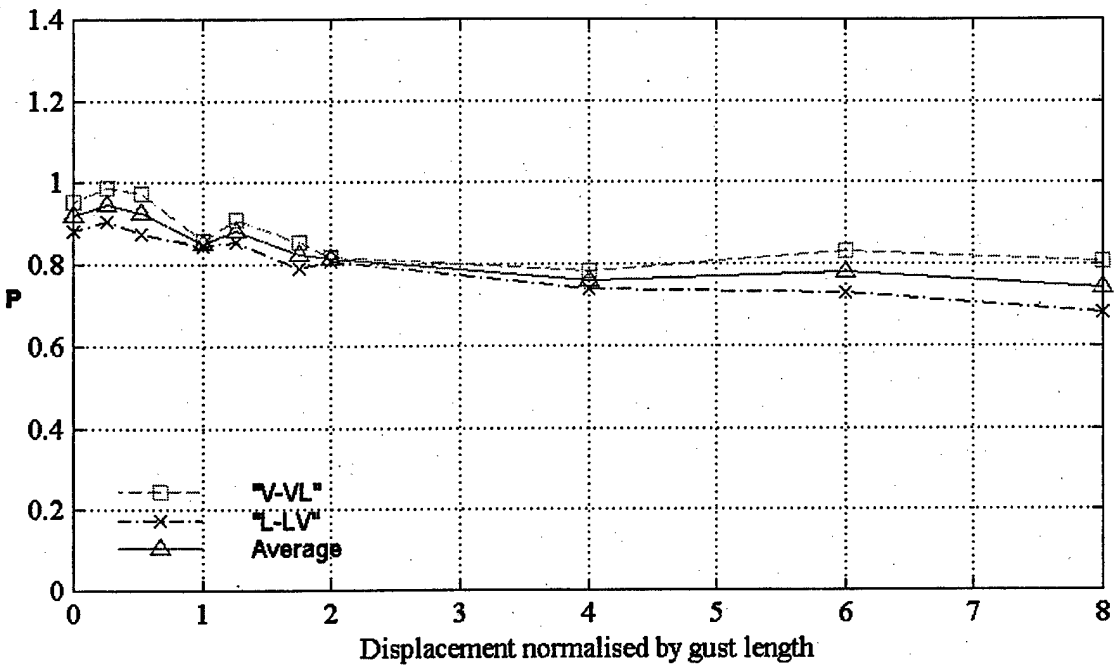

FIGURE 8. MEASURED VALUE OF AMPLITUDE-REDUCTION FACTOR *P*, AVERAGED OVER 25 RUNS, INCLUDING GUST COMPONENTS HAVING DIFFERENT GRADIENT DISTANCES. Average of results for H1 = 80 m from figure 7.

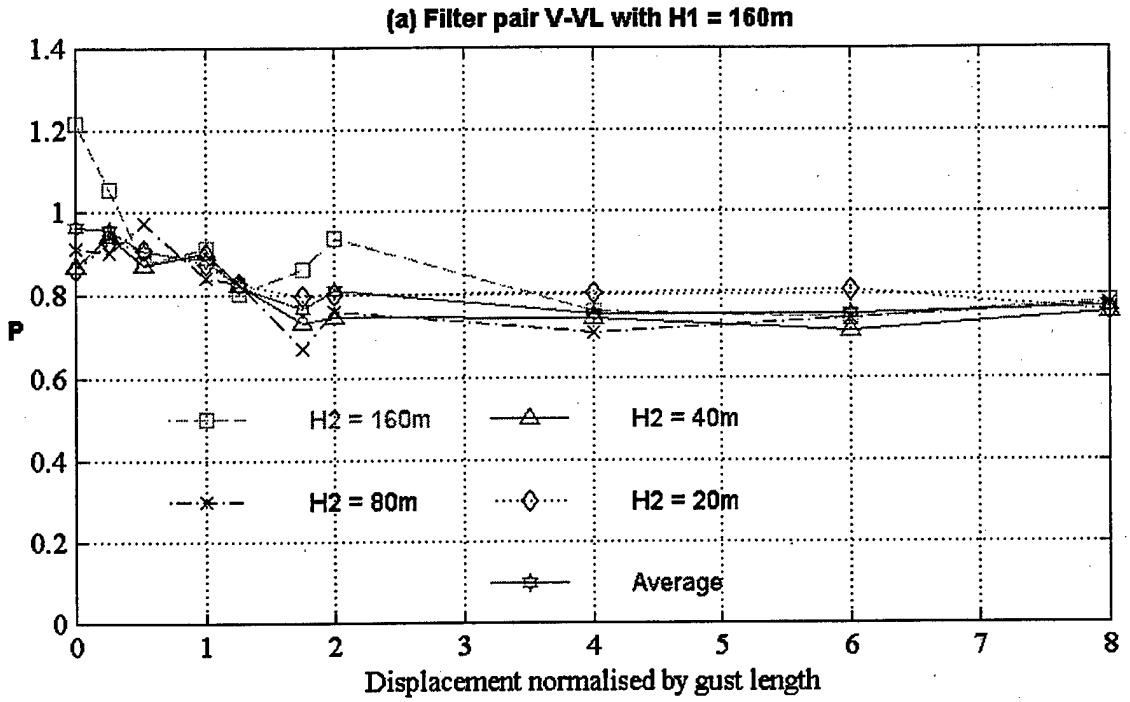

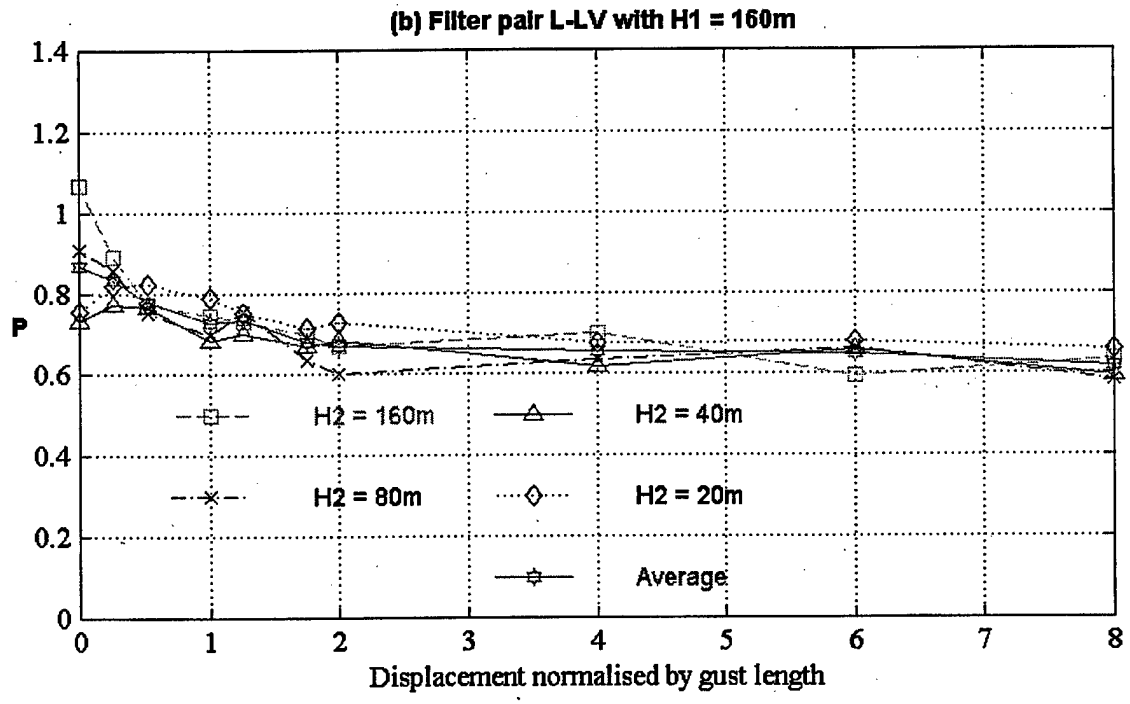

FIGURE 9. MEASURED VALUE OF AMPLITUDE-REDUCTION FACTOR *P*, AVERAGED OVER 25 RUNS, INCLUDING GUST COMPONENTS HAVING DIFFERENT GRADIENT DISTANCES, H1 = 160 m

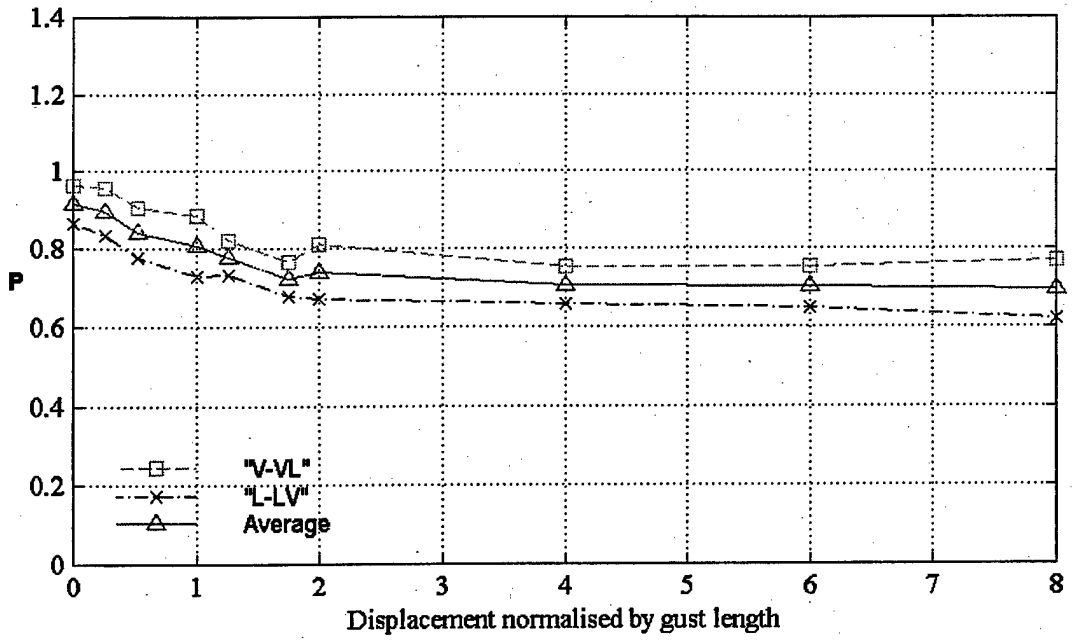

FIGURE 10. MEASURED VALUE OF AMPLITUDE-REDUCTION FACTOR *P*, AVERAGED OVER 25 RUNS, INCLUDING GUST COMPONENTS HAVING DIFFERENT GRADIENT DISTANCES. Average of results for H1 = 160 m from figure 9.

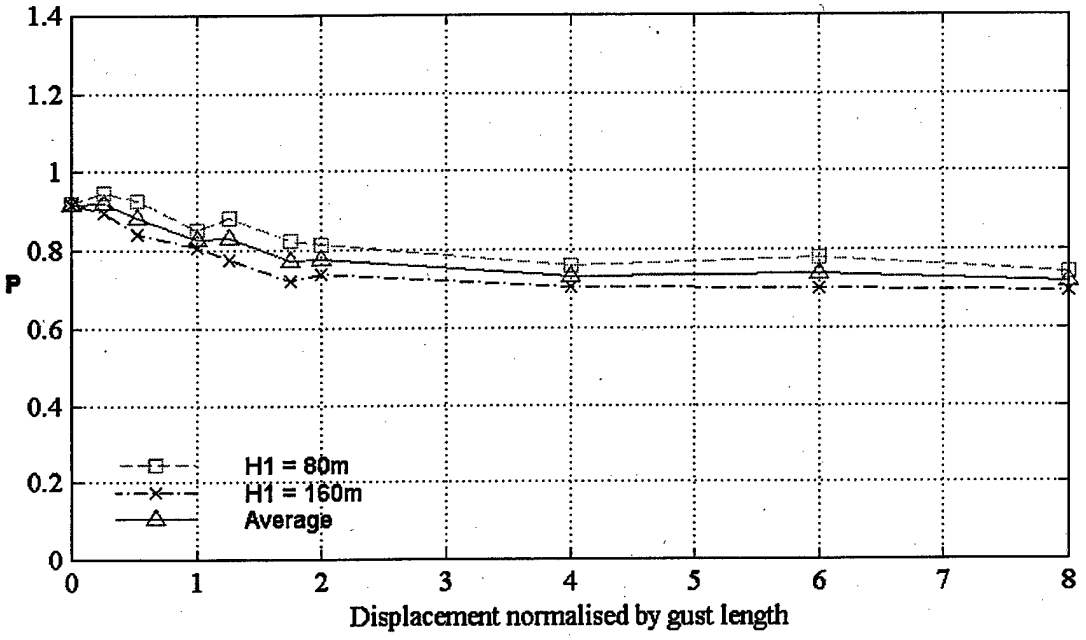

FIGURE 11. MEASURED VALUE OF AMPLITUDE-REDUCTION FACTOR *P*, AVERAGED OVER 25 RUNS, INCLUDING GUST COMPONENTS HAVING DIFFERENT GRADIENT DISTANCES. Average of results for H1 = 80 m and H1 = 160 m from figures 8 and 10.

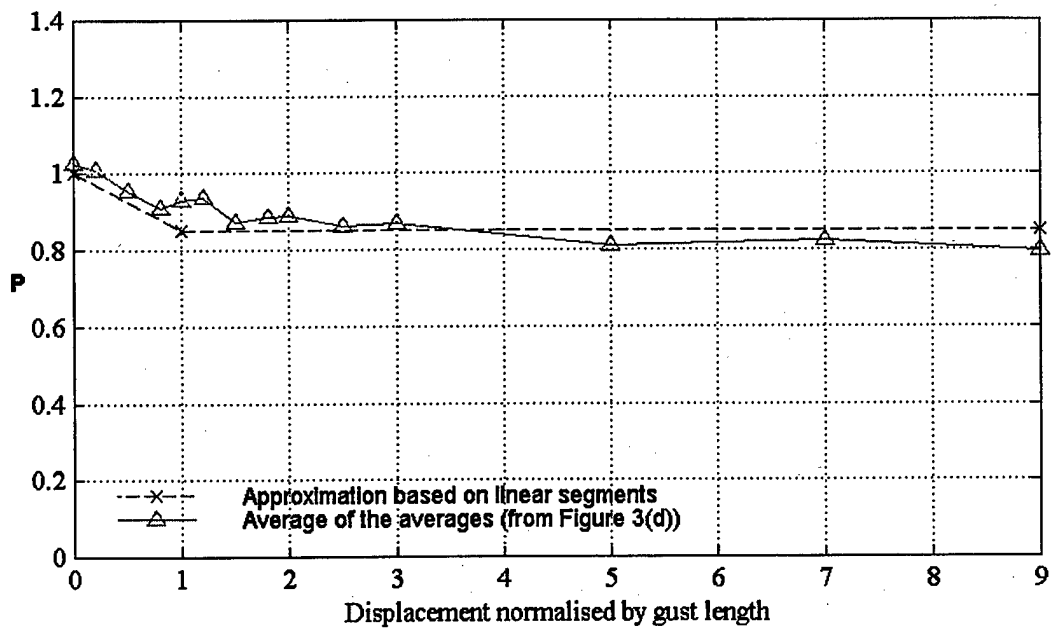

FIGURE 12. APPROXIMATION TO MEASURED AMPLITUDE-REDUCTION FACTOR *P* USING LINEAR-SEGMENTS, GUST COMPONENTS HAVING SAME GRADIENT DISTANCE

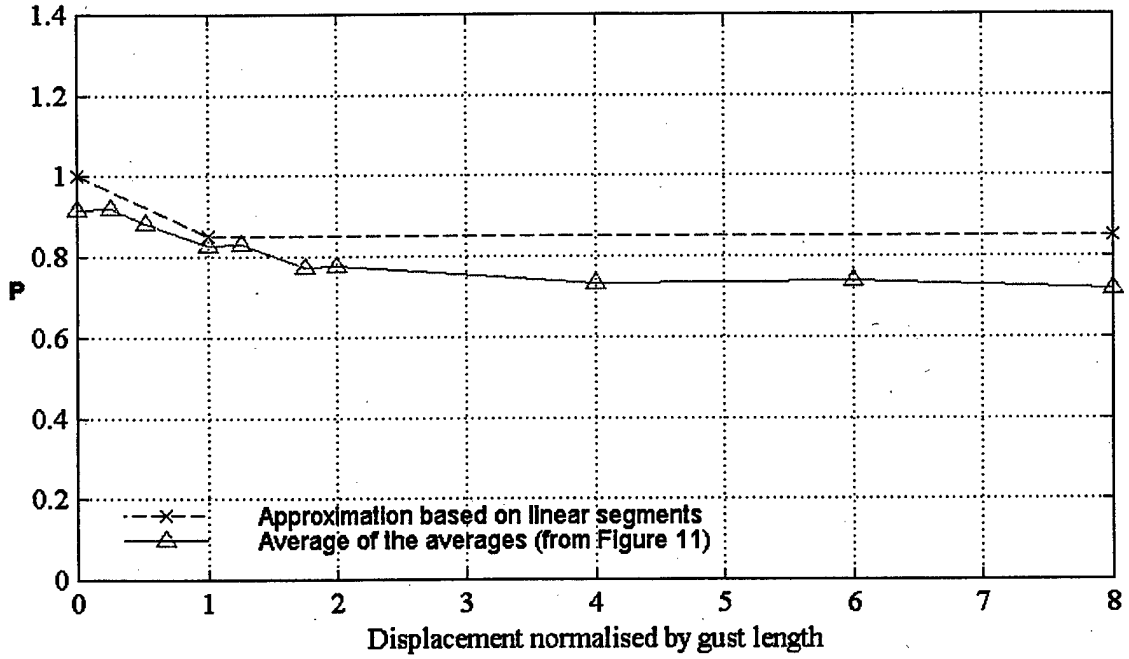

FIGURE 13. APPROXIMATION TO MEASURED AMPLITUDE-REDUCTION FACTOR *P* USING LINEAR-SEGMENTS, INCLUDING GUST COMPONENTS HAVING DIFFERENT GRADIENT DISTANCES

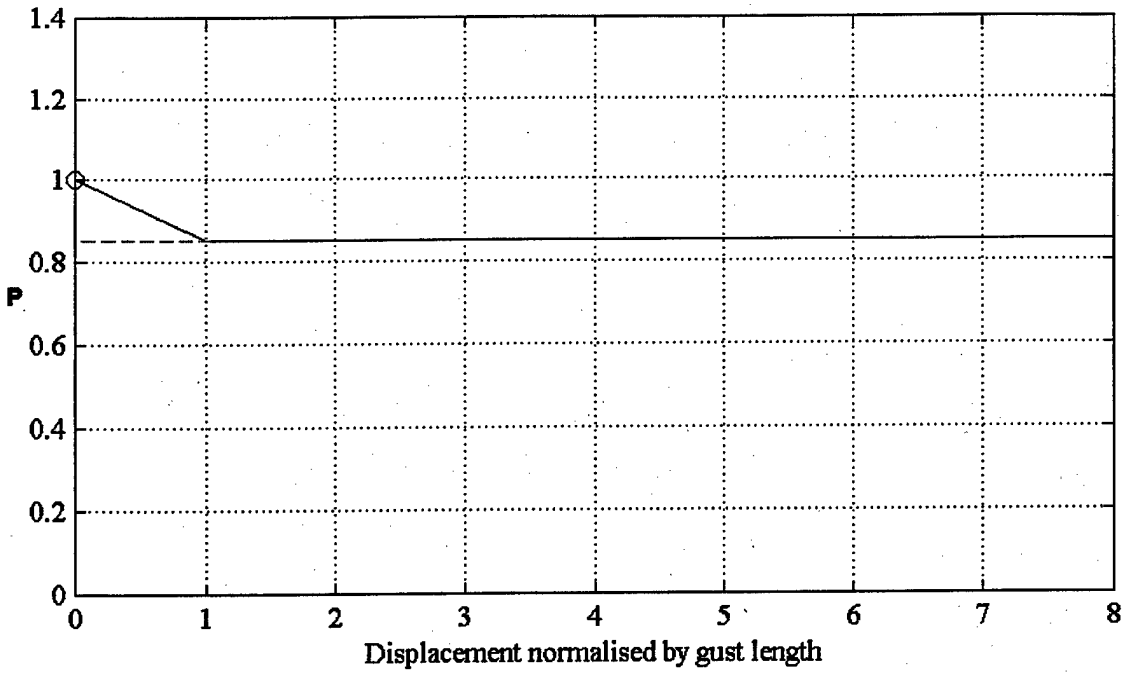

FIGURE 14. RELATIONSHIP BETWEEN LINEAR-SEGMENT APPROXIMATION (SOLID LINE) AND PROPOSED REQUIREMENT INCORPORATING AMPLITUDE-REDUCTION FACTOR *P*

Proposed requirement comprises P = 0.85 for all normalised displacements (including dashed line) together with P = 1 when gust components have same length and displacement = 0 (equivalent to round-the-clock).

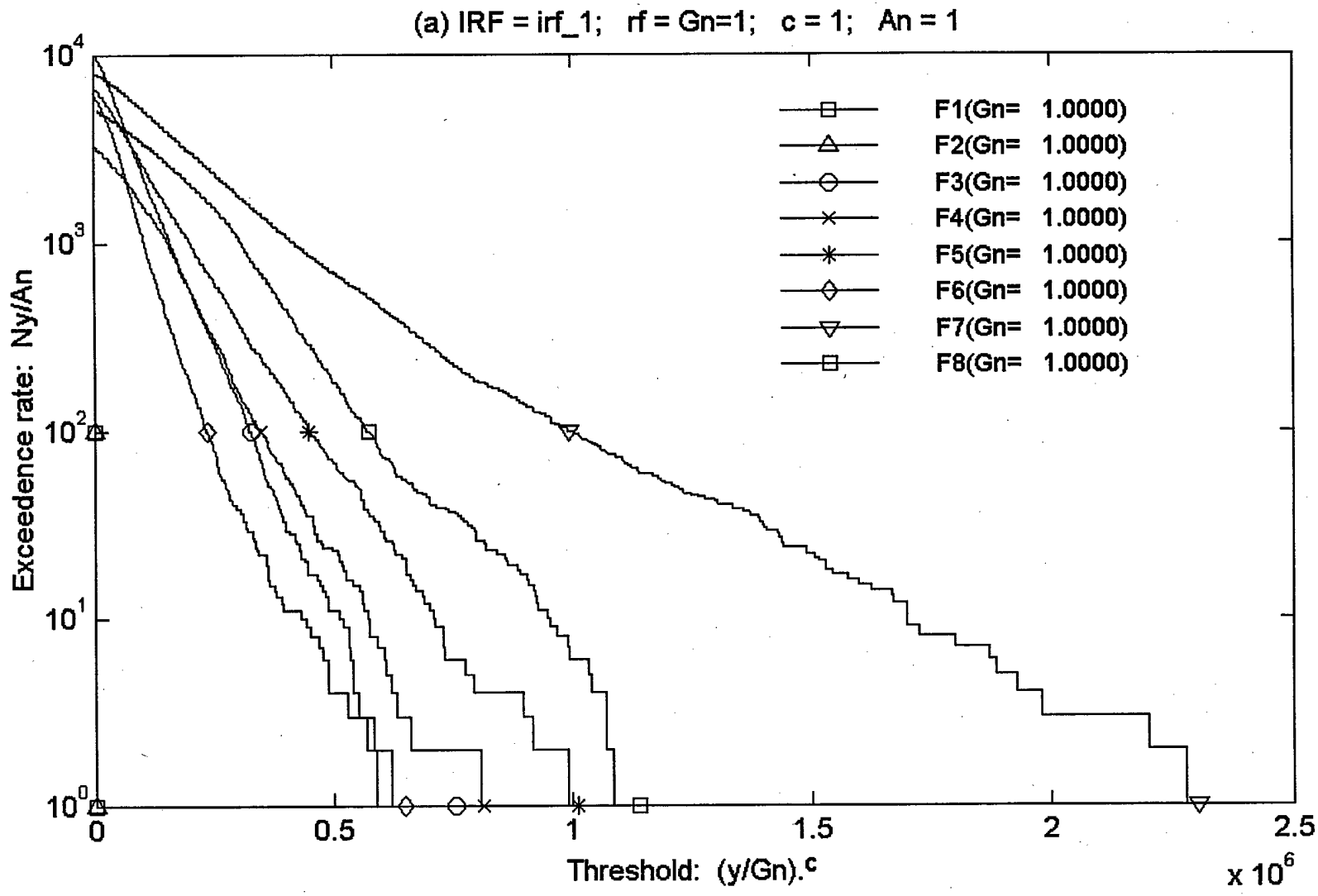

FIGURE 15a. THRESHOLD EXCEEDANCE PLOTS OF RESPONSE TO MULTIAXIS TURBULENCE, FLIGHT CASE 1 UNNORMALISED PLOTS

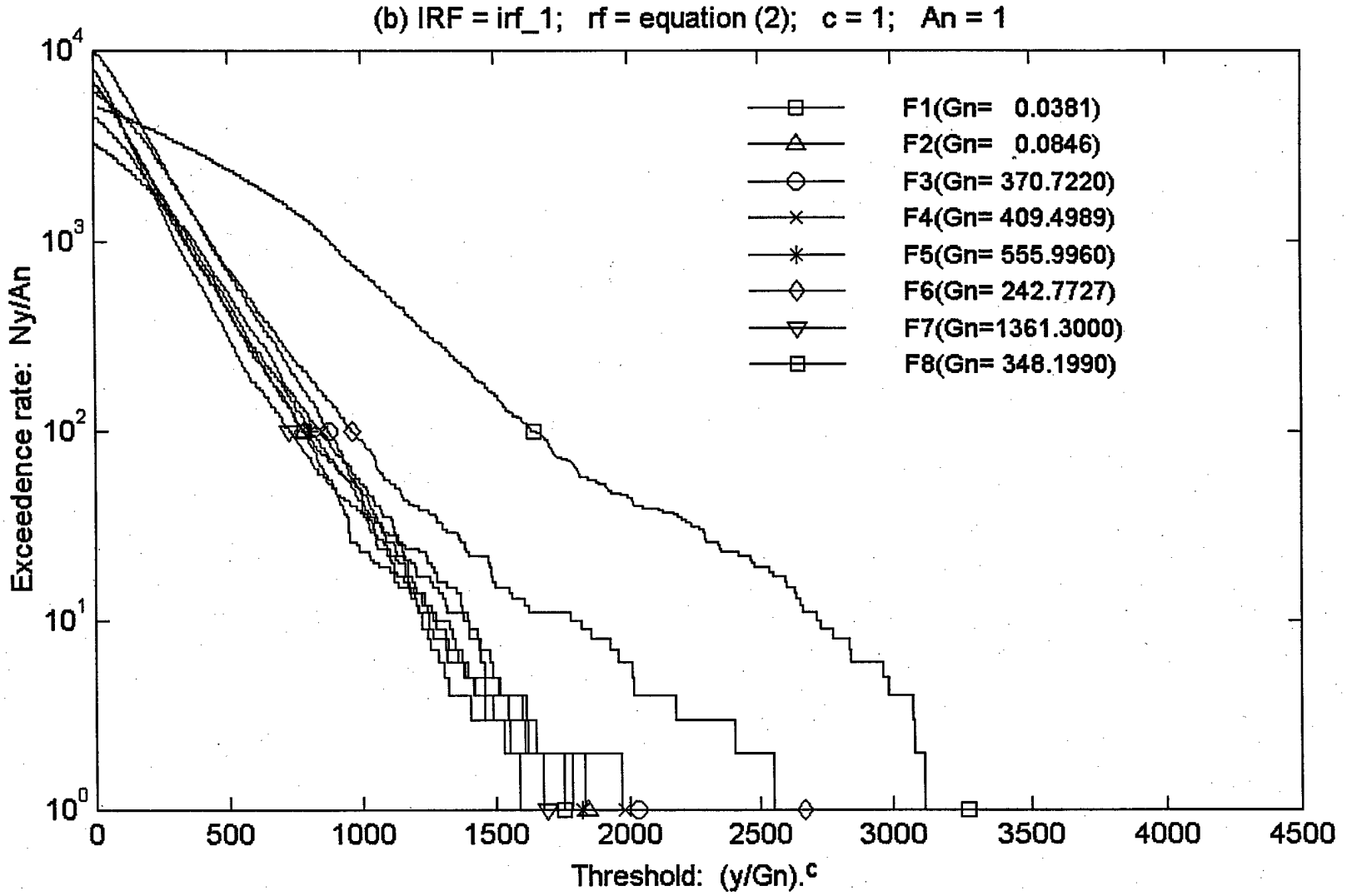

FIGURE 15b. THRESHOLD EXCEEDANCE PLOTS OF RESPONSE TO MULTIAXIS TURBULENCE, FLIGHT CASE 1 PLOTS NORMALISED USING EQUATION 2

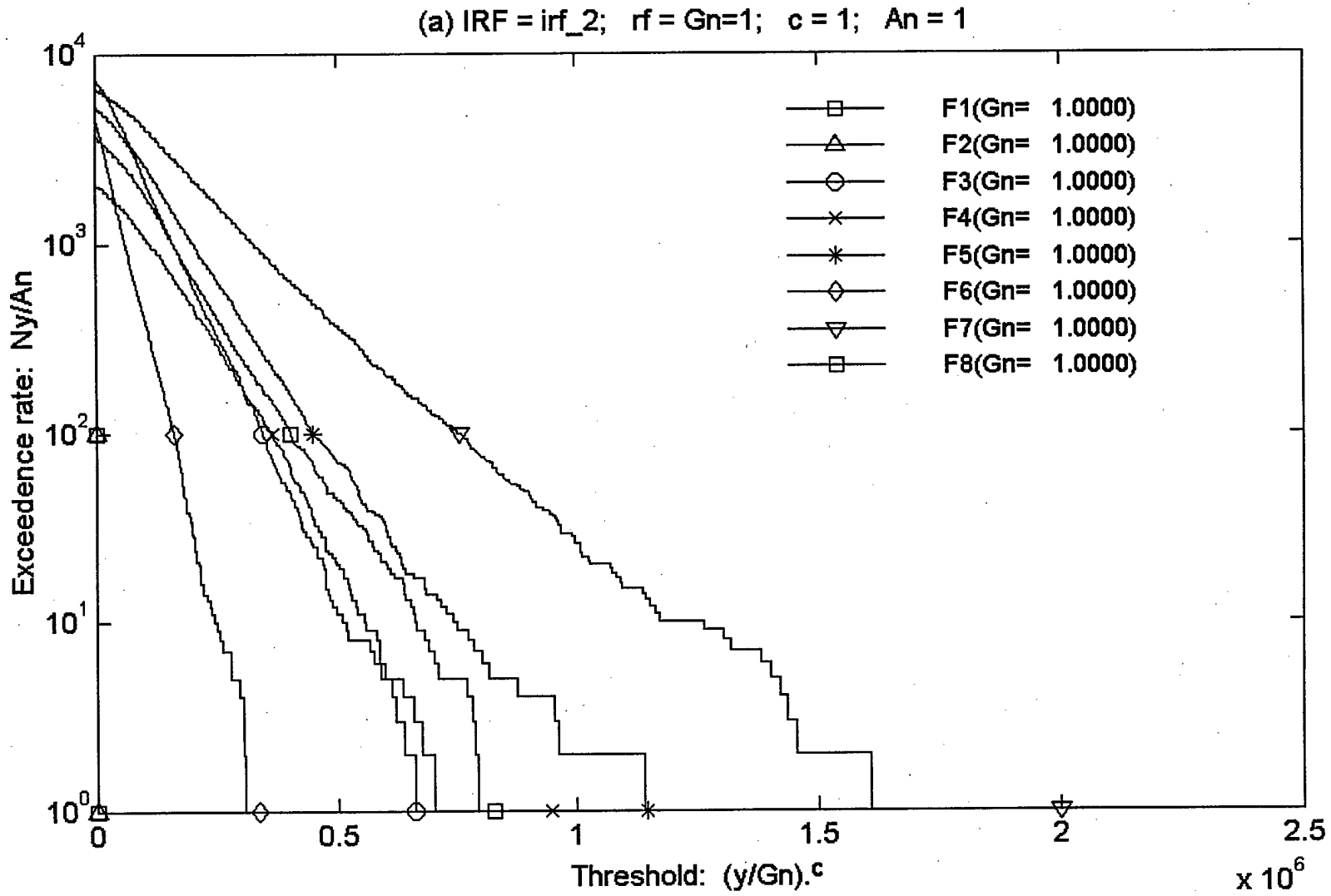

FIGURE 16a. THRESHOLD EXCEEDANCE PLOTS OF RESPONSE TO MULTIAXIS TURBULENCE, FLIGHT CASE 2 UNNORMALISED PLOTS

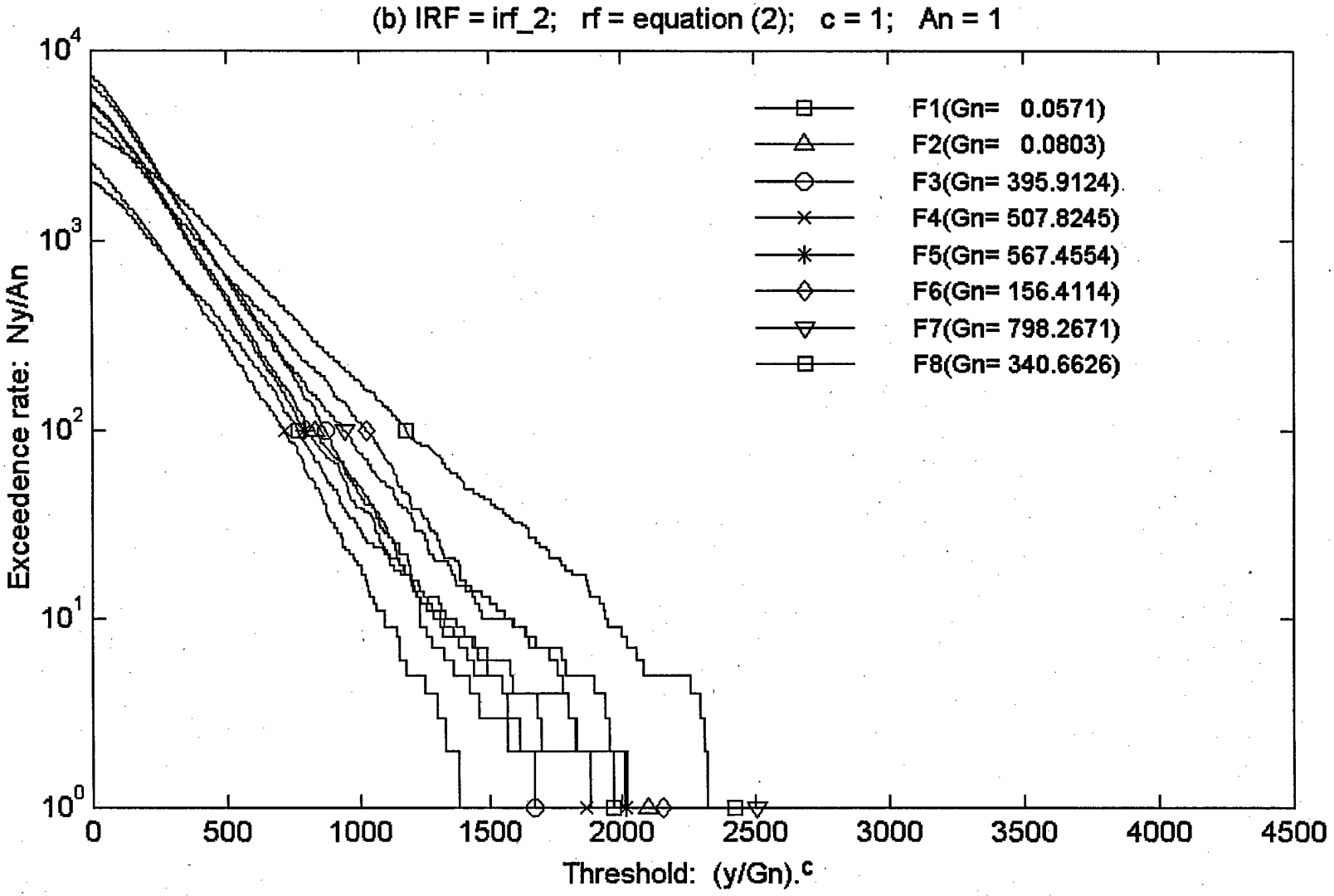

FIGURE 16b. THRESHOLD EXCEEDANCE PLOTS OF RESPONSE TO MULTIAXIS TURBULENCE, FLIGHT CASE 2
PLOTS NORMALISED USING EQUATION 2

TABLE 1. COMPARISON BETWEEN MULTIAXIS LOADS AND LOADS RESULTING FROM ISOLATED DISCRETE GUST IN A SINGLE AXIS (AIRBUS-TYPE MATHEMATICAL MODEL)

Flight Case 1: sea level, *Vc Mach=0.499*, high weight, *Vtas=169.8 m/s*

	Load			
Quantity (Section 10)	Isolated Vertical Load x_1	Isolated Lateral Load x_2	(Equation 2) $\sqrt{x_1^2 + x_2^2}$	Multiaxis Load $P.\sqrt{x_1^2 + x_2^2}$ $(P = 0.85)$
1	0.0293	0.0243	0.0381	0.0324
2	0.0583	0.0614	0.0846	0.0719
3	253.14	270.84	370.72	315.11
4	375.94	162.34	409.50	348.08
5	340.32	439.68	556.00	472.60
6	169.93	173.39	242.77	206.35
7	1302.4	396.32	1361.3	1157.1
8	196.38	287.80	348.42	296.16

Flight Case 2: 25000 ft, *Vc Mach=0.76*, low weight, *Vtas=237 m/s*

	Load			
Quantity (Section 10)	Isolated Vertical Load x_1	Isolated Lateral Load x_2	(Equation 2) $\sqrt{x_1^2 + x_2^2}$	Multiaxis Load $P.\sqrt{x_1^2 + x_2^2}$ $(P = 0.85)$
1	0.0526	0.0224	0.0571	0.0485
2	0.0593	0.0541	0.0803	0.0683
3	342.47	198.64	395.91	336.52
4	479.27	167.89	507.82	431.65
5	415.52	386.46	567.46	482.34
6	123.93	95.42	156.41	132.95
7	735.55	310.16	798.27	678.53
8	272.73	204.13	340.66	289.56

TABLE 2. COMPARISON BETWEEN MULTIAXIS LOADS AND LOADS RESULTING FROM ROUND-THE-CLOCK ANALYSIS (AIRBUS-TYPE MATHEMATICAL MODEL)

Flight Case 1: sea level, *Vc Mach=0.499*, high weight, *Vtas=169.8 m/s*

	Load	
Quantity (Section 10)	Round-The-Clock Load	Multiaxis Load $P\cdot\sqrt{x_1^2+x_2^2}$ *(P = 0.85)*
1	0.0315	0.0324
2	0.0623	0.0719
3	338.02	315.11
4	399.11	348.08
5	448.56	472.60
6	176.58	206.35
7	1302.4	1157.1
8	313.01	296.16

Flight Case 2: 25000 ft, *Vc Mach=0.76*, low weight, *Vtas=237 m/s*

	Load	
Quantity (Section 10)	Round-The-Clock Load	Multiaxis Load $P\cdot\sqrt{x_1^2+x_2^2}$ *(P = 0.85)*
1	0.0546	0.0485
2	0.0593	0.0683
3	348.02	336.52
4	485.93	431.65
5	415.52	482.34
6	124.30	132.95
7	737.16	678.53
8	293.58	289.56

TABLE 3. PERCENTAGE INCREASE IN LOAD IN GOING FROM WORST-CASE SINGLE AXIS TO MULTIAXIS CASE (AIRBUS-TYPE MATHEMATICAL MODEL)

Flight Case 1: sea level, *Vc Mach=0.499*, high weight, *Vtas=169.8 m/s*

Quantity (Section 10)	PSDMA	IDGRC	Tuned (1–cosine) in Each Axis (*P=0.85*)
1	38.2	7.51	10.58
2	16.4	1.47	17.10
3	26.0	24.80	16.35
4	39.7	6.16	0*
5	19.4	2.02	7.49
6	29.9	1.84	19.01
7	3.0	0.00	0*
8	7.1	8.76	2.90

Flight Case 2: 25000 ft, *Vc Mach=0.76*, low weight, *Vtas=237 m/s*

Quantity (Section 10)	PSDMA	IDGRC	Tuned (1–cosine) in Each Axis (*P=0.85*)
1	13.6	3.80	0*
2	14.1	0	15.18
3	9.8	1.62	0*
4	14.5	1.39	0*
5	15.6	0	16.08
6	36.4	0.30	7.28
7	4.0	0.22	0*
8	26.7	7.64	6.17

Note: 0* - zero (0) or load reduction

APPENDIX A—ILLUSTRATION OF METHOD OF MEASURING MULTIAXIS AMPLITUDE-REDUCTION FACTOR *P*

The method for measuring the amplitude-reduction factor *P* has been described in section 6.2. As explained, analysis of a given turbulence record using a gust pattern detection filter, related to a specified value of the gradient distance *L*, yields a measured statistical distribution, in the form of an exceedance rate *n(L,X)* of local extrema in filter outputs as a function of the threshold amplitude *X*. In terms of *n(L,X)*, the influence of energy-reduction factors is expressed by equation 19 from which the energy factor can be derived directly from the slope of a straight line fitted to a plot of *log{Ln(L,X)}* against *X*.

By applying this technique to the outputs of two filters, one (F1) designed to detect single (1-cosine) gusts and the other (F2) to detect pairs of such gusts (one in each of the vertical and lateral axes). Dividing the slope obtained for the gust pair by that obtained for the single (1-cosine) gust we obtain a measurement of the amplitude-reduction factor *P* from the ratio of the resulting slopes, equation 20. For convenience of presentation, the $\sqrt{2}$ factor in equation 20 has been absorbed as a factor in the output of filter F2 so that *P* is derived directly as a ratio of slopes.

The required slopes have been obtained by least-squares fitting of straight-line segments, over specified ranges of amplitude, to the measured exceedance rates *n(L,X)*, using log-linear axes. Examples of such measured exceedance rates, typical of those from which values of *P* have been derived in the present study, are illustrated in figures A-1 to A-6.

Each of these plots, figures A-1 to A-6, comprises six subplots in the form of two vertical columns of three subplots each. Each subplot contains two graphs, one corresponding to each filter, F1 and F2. The measured exceedance rates in each such column of three subplots are identical, the differences between the subplots in each group of three being only in the parameters by means of which the axes have been normalised. The significance of these normalising parameters, and of the other symbols used, is explained in the following.

As in section 11, the figures have been produced using a general-purpose analysis program for normalising log-linear plots of exceedance rates in which *y* is used to denote threshold amplitude and *Ny* is used to denote rate of exceedance of threshold *y*. For present purposes we make the identification:

$$y : X$$
$$Ny : n(L,X)$$

In these figures, the above variables are normalised in the form $(y/Pn)^c$ and *Ny/An*, where the subscript *n* refers to the respective filter: $n = 1$ for filter F1 and $n = 2$ for filter F2. Filter F1 is taken to be a datum filter, for which $Pn = 1$ and $An = 1$ $(Fn = 1)$. Values for *Pn* and *An* for the second filter, F2 $(Fn = 2)$, are different for each subplot of a vertical set of three and are tabulated within each subplot.

In the first subplot of each set of three, the values of *An* and *Pn* for $n = 2$ are derived by least-squares fitting of straight-line segments to the measured exceedance rates, over the ranges of amplitude between the pairs of symbols printed on the graphs—squares for F1 and triangles for F2 (note that the end points on each graph are similarly marked with symbols to assist in identification of the respective graphs). The success of the least-squares fitting process is confirmed by the fact that, in the first subplot, a straight line passing through the two squares is coincident with a straight line passing through the two triangles. It follows from the fact that the $\sqrt{2}$ factor in equation 20 has been absorbed as a factor in the output of filter F2 that the required amplitude-reduction factor $P = Pn$ when $n = 2$, the value of which is tabulated on the subplot.

Also tabulated on the first subplot is a value of An, derived from the least-squares fitting process and used in the normalisation of the exceedance-rate axis. This factor is analogous to the n-zero term in a PSD analysis and is not relevant to the measurement of *P*. The other quantities tabulated on the first subplot are sep and c. Sep refers to the gust component separation and, for reasons related to the sampling of the data, is expressed as a multiple of (gradient distance) / 5. c is used as an index in the normalisation of the threshold amplitude *(y/Pn)* and influences the curvature of the graphs, being chosen empirically so that they can be well fitted by a segment of straight line.

Subplots two and three, of a vertical set of related graphs, present the same data as the first subplot but normalised by a predetermined set of parameters *Pn* and *An* and are included so that the success of the normalisation used in the first subplot can be more easily assessed. In the second subplot, $Pn = 1$ and $An = 1$. In this case the divergence between the slopes of the plotted graphs confirms the need for an amplitude-reduction factor *P* less than unity. In the third subplot, nominal values $Pn = 0.85$ and $An = 1.7$ are used. The value $Pn = 0.85$ is based on the prediction that a value of $P = 0.85$ is to be expected as a typical value. The value $An = 1.7$ is a fixed nominal value based on a preliminary analysis of the data.

Figures A-1 to A-6 present a selection of results, in the form outlined above, for a range of filter combinations, such as V-LV, defined in section 7.1, a range of gradient distances H, and a range of gust-component separations sep. Plots in this form have been produced for every condition considered in the present analysis programme as part of the process of confirming the validity of the measured values of the amplitude-reduction factor *P*.

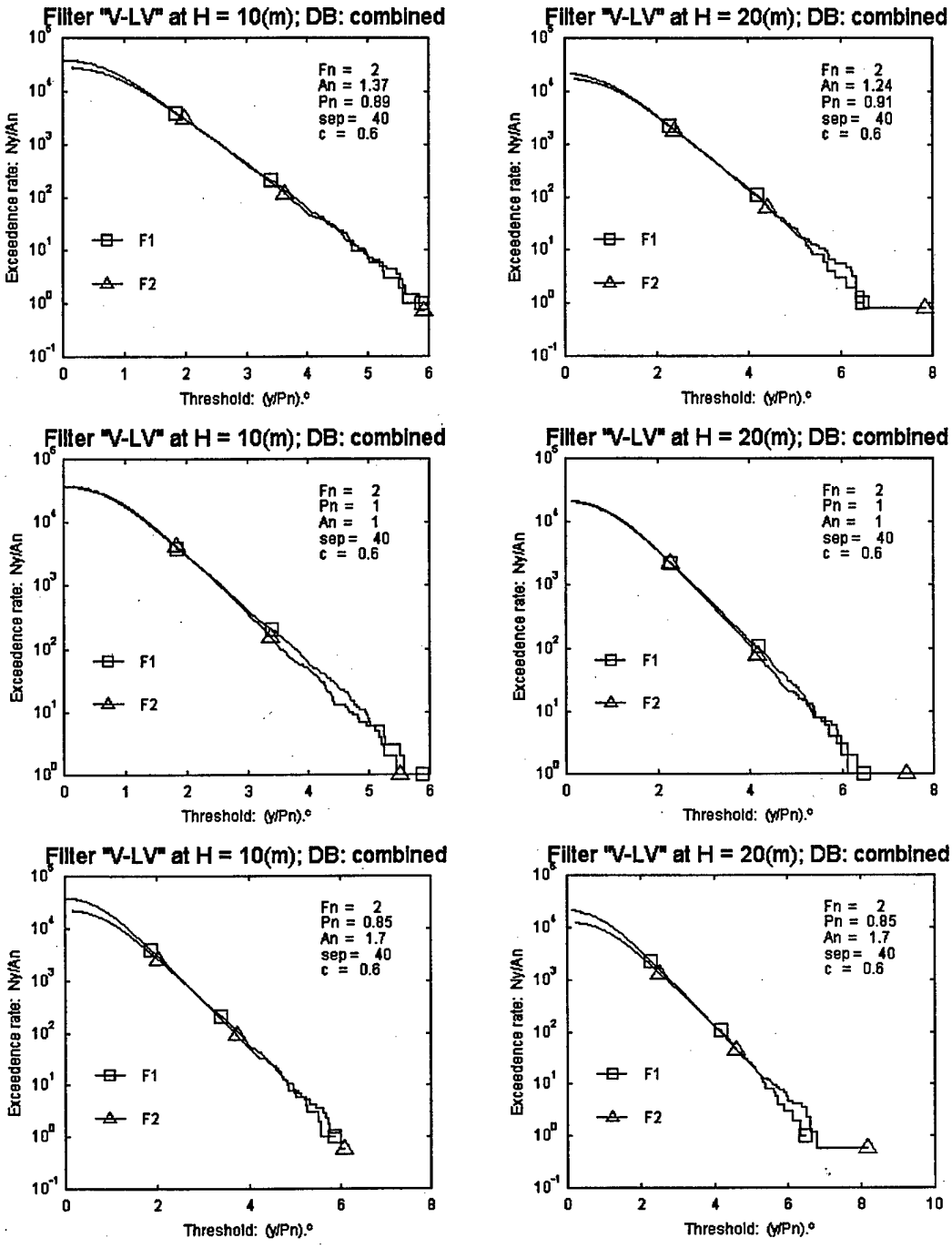

FIGURE A-1. MEASURED STATISTICAL DISTRIBUTIONS ILLUSTRATING METHOD OF MEASURING AMPLITUDE-REDUCTION FACTOR *P*
(See appendix A for description and nomenclature.)

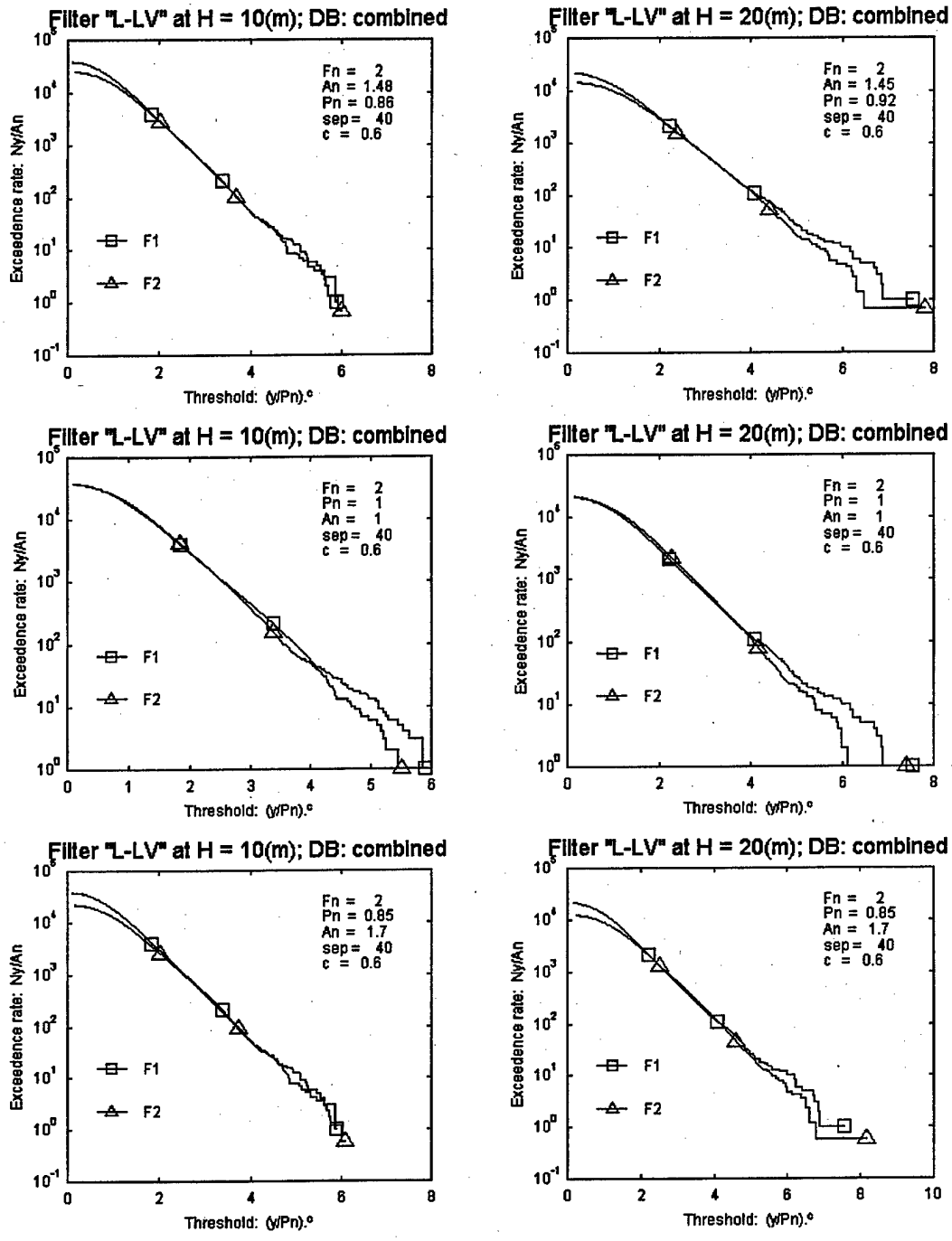

FIGURE A-2. MEASURED STATISTICAL DISTRIBUTIONS ILLUSTRATING METHOD OF MEASURING AMPLITUDE-REDUCTION FACTOR *P*
(See appendix A for description and nomenclature.)

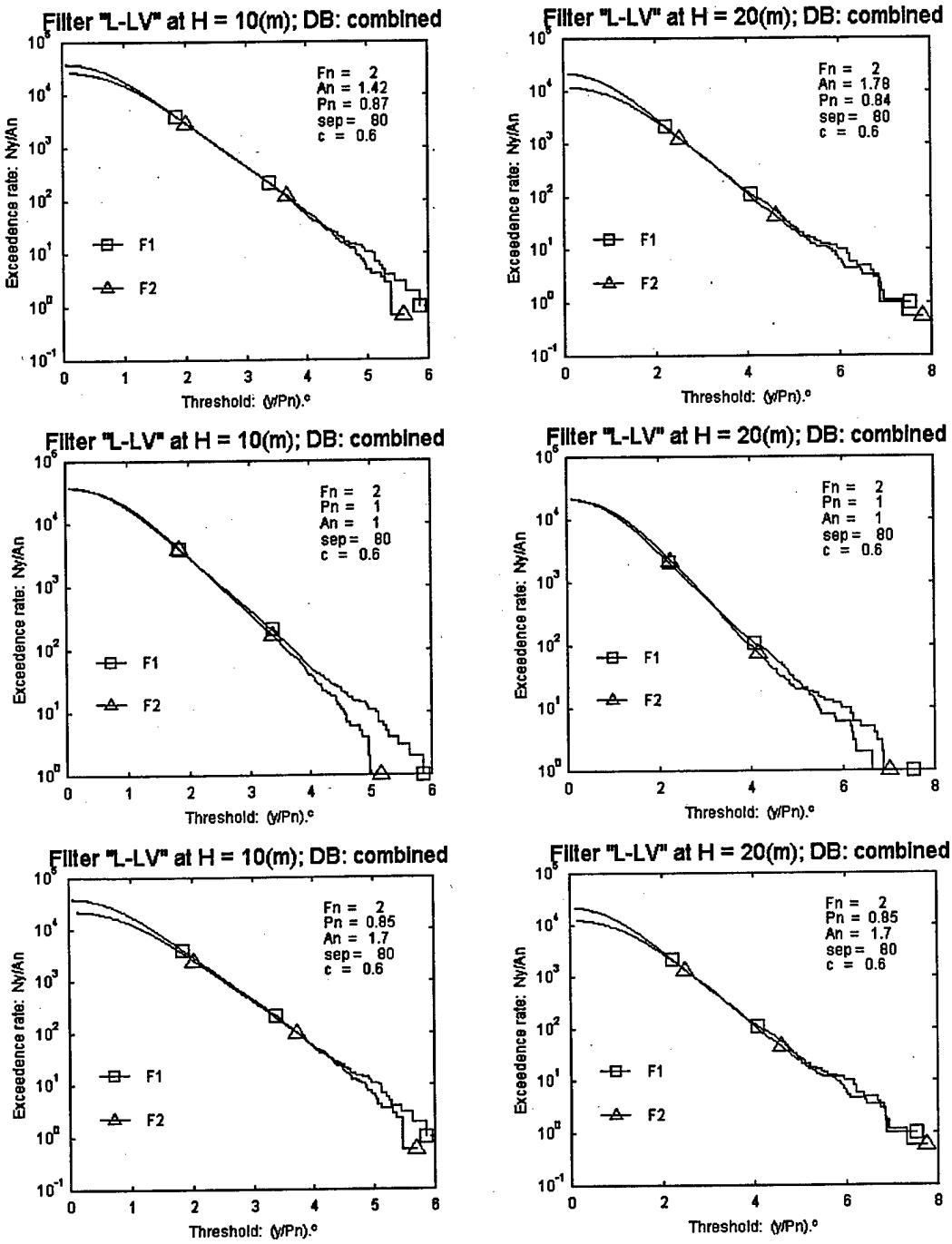

FIGURE A-3. MEASURED STATISTICAL DISTRIBUTIONS ILLUSTRATING METHOD OF MEASURING AMPLITUDE-REDUCTION FACTOR *P*
(See appendix A for description and nomenclature.)

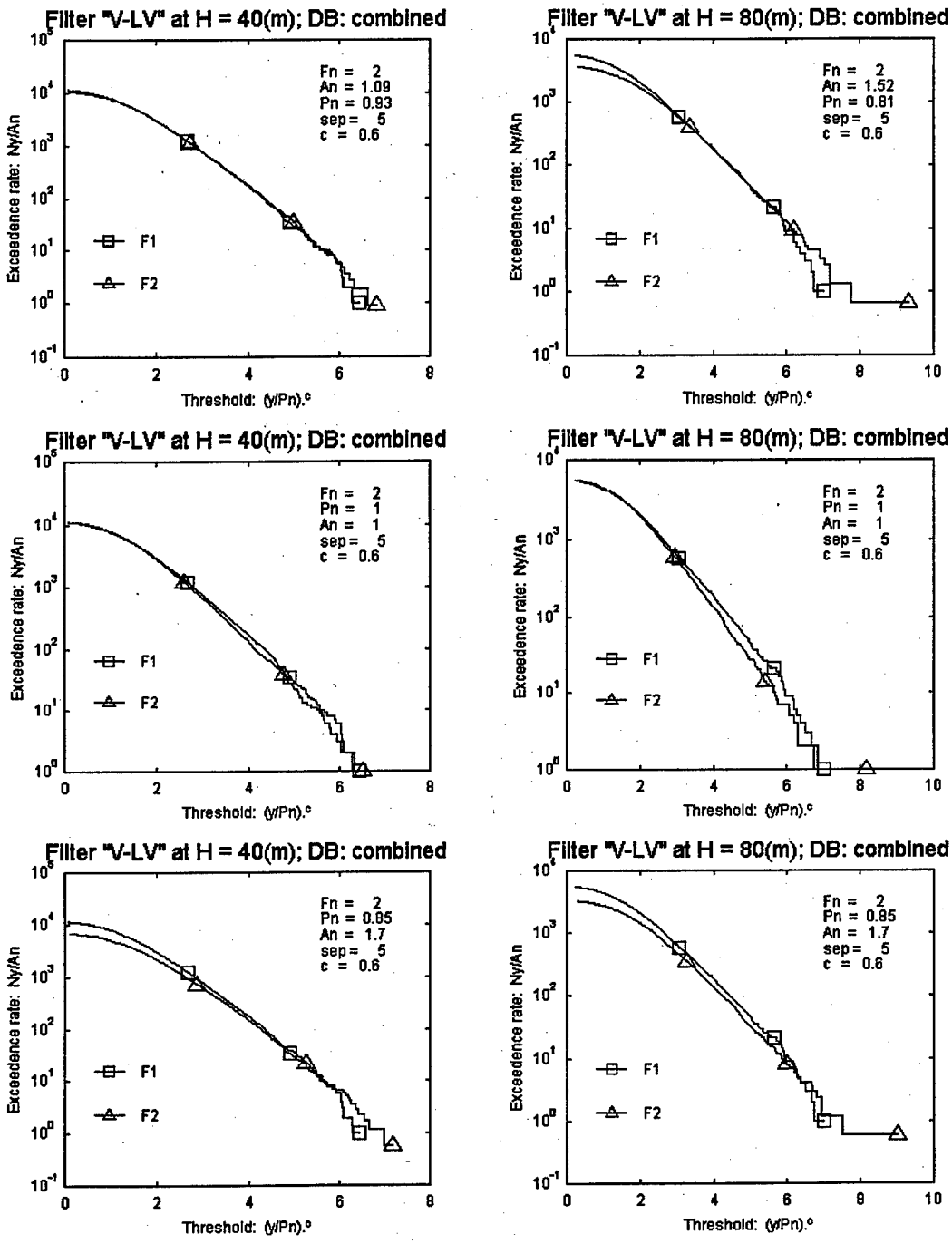

FIGURE A-4. MEASURED STATISTICAL DISTRIBUTIONS ILLUSTRATING METHOD OF MEASURING AMPLITUDE-REDUCTION FACTOR *P*
(See appendix A for description and nomenclature.)

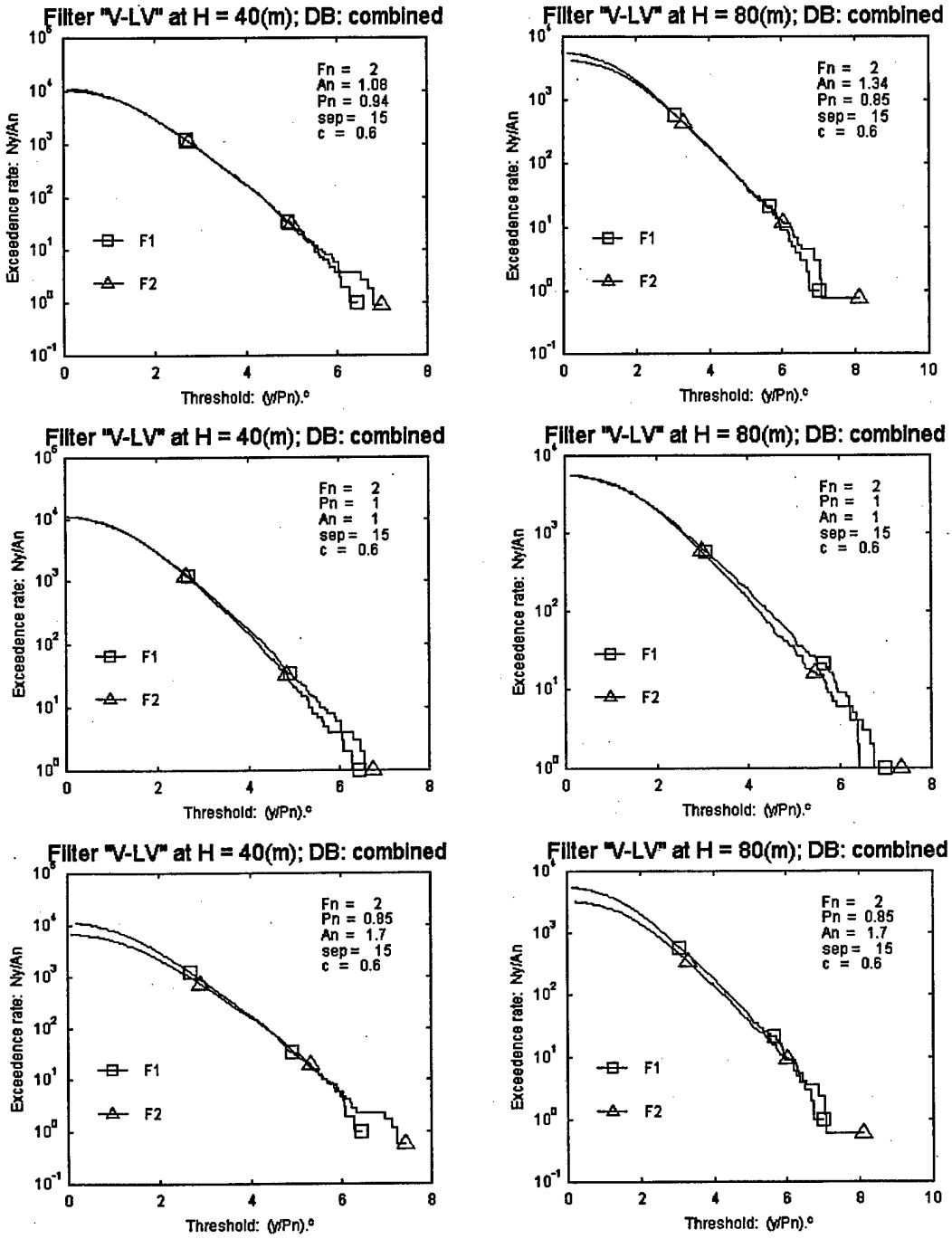

FIGURE A-5. MEASURED STATISTICAL DISTRIBUTIONS ILLUSTRATING METHOD OF MEASURING AMPLITUDE-REDUCTION FACTOR *P*
(See appendix A for description and nomenclature.)

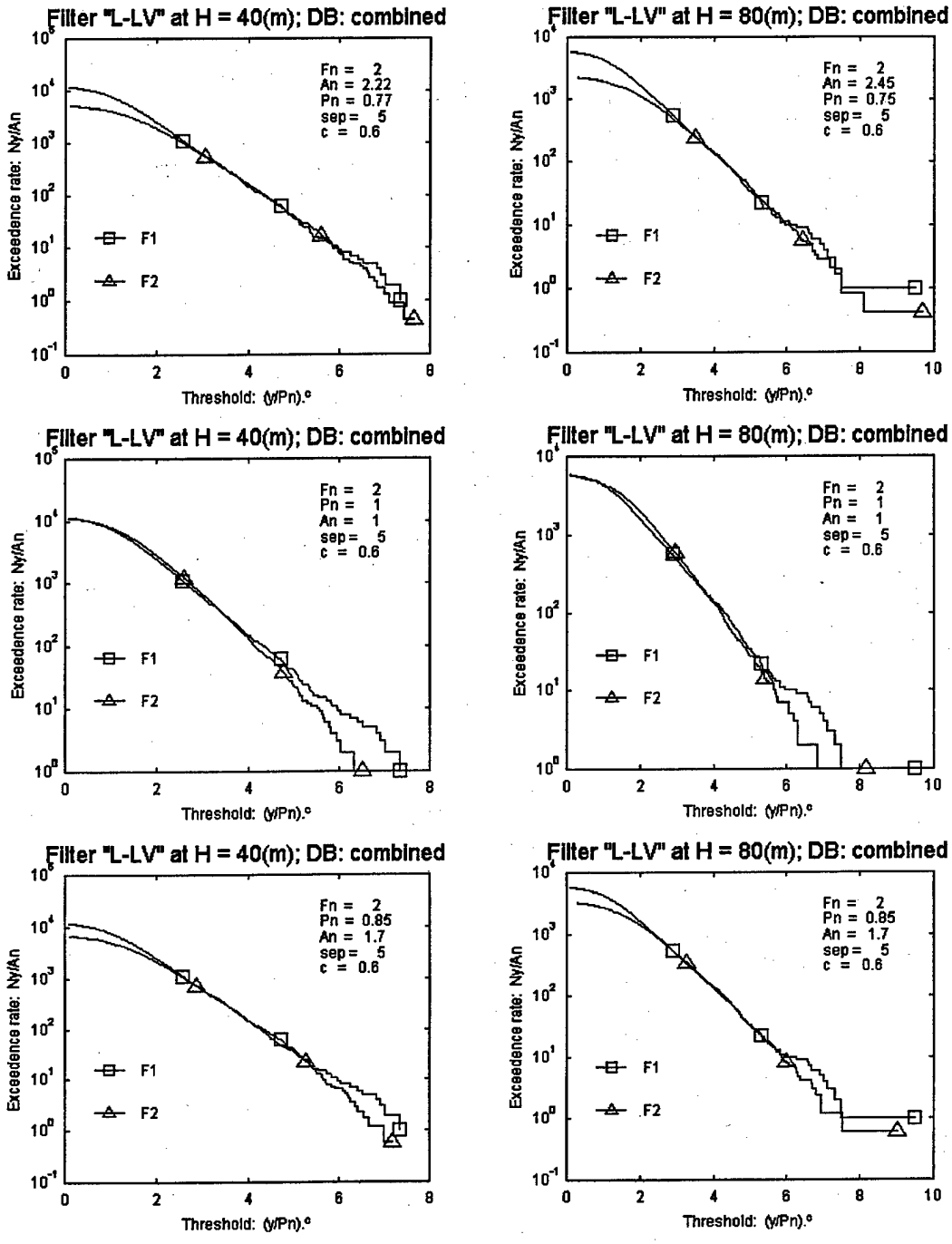

FIGURE A-6. MEASURED STATISTICAL DISTRIBUTIONS ILLUSTRATING METHOD OF MEASURING AMPLITUDE-REDUCTION FACTOR *P*
(See appendix A for description and nomenclature.)

APPENDIX B—GENERATION OF TIME-HISTORIES WITH RANDOMISED PHASE

As a means of checking the extent to which numerical results derived from the analysis of measured turbulence data depend upon the effects of phase correlation, a method has been developed for generating signals which have identical power spectral densities to the measured turbulence velocities but for which the phase is purely random.

The method involves taking the Fourier transform of the measured velocity component, retaining the *amplitude* component of this Fourier transform but replacing the measured *phase* component by a random-phase component, and finally applying an inverse Fourier transform to generate the required signal.

The MATLAB routine used to perform this transformation is as follows:

```
% randomise phase.  Input: sig1;  Output: sig2.

x=fft(sig1);
temp=exp(2*pi*i*rand(1,(length(x)-2)/2));
ph=[1,temp,1,conj(temp(length(temp):-1:1))]';
x2=abs(x).*ph;
sig2=real(ifft(x2));
```